ESCAP/WMO
Typhoon Committee

Available online at www.sciencedirect.com

ScienceDirect

Tropical Cyclone Research and Review 10 (2021) 125–150

www.keaipublishing.com/tcrr

Estimating tropical cyclone surface winds: Current status, emerging technologies, historical evolution, and a look to the future

John A. Knaff [a,*], Charles R. Sampson [b], Matthew E. Kucas [c], Christopher J. Slocum [a], Michael J. Brennan [d], Thomas Meissner [e], Lucrezia Ricciardulli [e], Alexis Mouche [f], Nicolas Reul [f], Mary Morris [g], Galina Chirokova [h], Philippe Caroff [i]

[a] *NOAA/Center for Satellite Applications and Research, Fort Collins, CO, USA*
[b] *Naval Research Laboratory, Monterey, CA, USA*
[c] *Joint Typhoon Warning Center, Pearl Harbor, Hawaii, USA*
[d] *NOAA/NWS/NCEP National Hurricane Center, Miami, FL, USA*
[e] *Remote Sensing Systems, Santa Rosa, CA, USA*
[f] *Ifremer, Univ. Brest, CNRS, IRD, Laboratoire d'Océanographie Physique et Spatiale, IUEM, 29280 Brest, France*
[g] *NASA/Jet Propulsion Laboratory, Pasadena, CA, USA*
[h] *Cooperative Institute for Research in the Atmosphere, Fort Collins, CO, USA*
[i] *Tropical Cyclone/Regional Specialized Meteorological Center, Météo France, Réunion, France*

Available online 17 September 2021

Abstract

This article provides a review of tropical cyclone (TC) surface wind estimation from an operational forecasting perspective. First, we provide a summary of operational forecast center practices and historical databases. Next, we discuss current and emerging objective estimates of TC surface winds, including algorithms, archive datasets, and individual algorithm strengths and weaknesses as applied to operational TC surface wind forecast parameters. Our review leads to recommendations about required surface coverage − an area covering at least 1100 km from center of TC at a 2-km resolution in the inner-core, and at a frequency of at least once every 6 h. This is enough coverage to support a complete analysis of the TC surface wind field from center to the extent of the 34-kt (17 m s^{-1}) winds at 6-h intervals. We also suggest future designs of TC surface wind capabilities include funding to ensure near real-time data delivery to operators so that operational evaluation and use are feasible within proposed budgets. Finally, we suggest that users of archived operational wind radii datasets contact operational organizations to ensure these datasets are appropriate for their needs as the datasets vary in quality through time and space, even from a single organisation.

Keywords: Tropical cyclone; Surface wind; Satellite; Best track; Operations

1. Introduction

Tropical Cyclones (TCs, also see Table 1 for this and all other acronyms) come in a variety of intensities and sizes (Chavas and Emanuel, 2010; Knaff et al., 2014). Because of this variability, TC near-surface winds as captured by the integrated size and magnitude (i.e., kinetic energy) determine the destructive potential (Powell and Reinhold, 2007) and drive storm surge (Needham and Keim, 2014; Irish et al.,

* Corresponding author.
E-mail address: john.knaff@noaa.gov (J.A. Knaff).
Peer review under responsibility of Shanghai Typhoon Institute of China Meteorological Administration.

ELSEVIER Production and hosting by Elsevier on behalf of KeAi

https://doi.org/10.1016/j.tcrr.2021.09.002

Table 1
A list of acronyms used in this paper along with brief definitions.

Acronym	Definition
AMSR2	Advanced Microwave Scanning Radiometer-2
ASCAT	Advanced Scatterometer
ATCF	Automated Tropical Cyclone Forecast System
CARQ	Combined Automated Request Query (in ATCF)
COM	Communications line (in ATCF)
CPHC	Central Pacific Hurricane Center
CYGNSS	Cyclone Global Navigation Satellite System
ERS (1 and 2)	European Remote Sensing Satellite
ESA	European Space Agency
EUMETSAT	European Organisation for the Exploitation of Meteorological Satellites
GEMS	Global Environmental Monitoring System
GMF	Geophysical Model Function
GNSS-R	Global Navigation Satellite System Reflectometry
GPS	Global Positioning System
HRD	NOAA's Hurricane Research Division
HURDAT2	Hurricane Database-2
HY-2A	Haiyang (ocean)-2A
HSCAT	HY-2 Scatterometer
IFREMER	Institut Français de Recherche pour l'Exploitation de la Mer
IR	Infrared (digital imagery)
JTWC	Joint Typhoon Warning Center
KMNI	Koninklijk Nederlands Meteorologisch Institute
kt	nautical miles per hour
Metop	Meteorological Operational satellite
NHC	National Hurricane Center
NSCAT	NASA Scatterometer
QuikScat	Quick Scatterometer
R30	Maximum radial extent of 30 knot winds (in quadrants)
R34	Maximum radial extent of 34 knot winds (in quadrants)
R50	Maximum radial extent of 50 knot winds (in quadrants)
R64	Maximum radial extent of 64 knot winds (in quadrants)
RapidScat	Rapid Scatterometer
RCM	RadarSat Constellation Mission
RSS	Remote Sensing Systems
RMW	Radius of Maximum Wind
ROCI	Radius of Outermost Closed Isobar
RSME	Root Mean Square Error
RSMC	Regional Specialized Meteorological Centre
SATCON	Satellite (intensity) Consensus
SCATSAT	Scatterometer Satellite
SFMR	Stepped Frequency Microwave Radiometer
SMAP	Soil Moisture Active Passive
SNPP	Suomi National Polar-orbiting Partnership satellite
SMOS	Soil Moisture Ocean Salinity
SSM/I	Special Sensor Microwave Imager
SSMIS	Special Sensor Microwave Imager/Sounder
TC	Tropical Cyclone
TROPICS	Time-Resolved Observations of Precipitation structure and storm Intensity with a Constellation of SmallSats
VMAX	One-minute maximum sustained wind or intensity
WSF-M	U.S. Air Force's Weather System Follow-on Mission

2008). Thus, warning centers must accurately estimate and distribute TC surface wind strength for public warnings and risk mitigation in real time. Operational TC wind field estimates have evolved in quality and continue to evolve with improvements in the measurements and algorithms to derive the winds. Operational TC surface wind analyses benefit from some new capabilities, but the capabilities have caveats. Consequently, the evolutions to and capabilities for wind field estimation require documentation.

In this review, we aim to enable readers with information regarding the best use of operational center TC surface wind analyses, historical or climatological datasets, and TC-specific surface wind data currently or soon to be available to operational centers. We define various types of TC surface wind estimates used at the forecast centers, and provide a history of operational practices. Then, we discuss the tools available for assessing TC surface winds, and summarize objective datasets available to researchers for climatological and application

development studies. Throughout this review, we use knots (kts, 1 kt = 0.51444 m s^{-1}) as the wind speed unit to be consistent with operational centers. Also, we note that our review complements recent reviews on remote sensing of oceanic surface winds (Bourassa et al., 2019) and of ocean observations (Domingues et al., 2019). For brevity, our review does not detail TC intensity estimation techniques (Dvorak, 1984; Brueske and Velden, 2003; Demuth et al., 2004; Velden et al., 2006; Herndon and Velden, 2014; Olander and Velden, 2019; Wimmers et al., 2019; Velden and Herndon, 2020), but does recognize their applicability for determining TC surface wind magnitude.

TC surface winds, and marine or overland exposures to winds at 10-m elevations, are often defined in terms of the time-averaged magnitude of the wind speeds. To represent the TC vortex, the winds are categorized as maximum winds or intensity (VMAX), the radius of maximum winds (RMW), and radii associated with maximum radial extent of wind speed thresholds, like 64-, 50-, 34-kt (R64, R50, R34) over a portion of the storm circulation. Quantities like R34, R50, and R64 are collectively referred to as "wind radii", and are most often provided in geographic quadrants. TC warning agencies include VMAX and the wind radii in forecast advisories (e.g., NHC, 2020; OFCM, 2019) issued by; noting that advisory format varies between these agencies. TC warning centers also evaluate data available in real-time to formulate subjective estimates of wind characteristics for their operational customers. Surface wind data estimates available within 2 h and 4 h of synoptic time are considered "real time", and "operationally available", respectively and hereafter. This terminology is adopted because TC warning centers provide these estimates at synoptic times (every 6 h at 00, 06, 12 and 18 UTC) as part of the advisory/forecast cycle issued within 3 h of the synoptic time. These estimates form the basis for the subjectively analyzed TC location, intensity, and wind radii over the TC lifetime—a data record commonly referred to as a "best track", discussed in section 2.

TC surface winds methods vary considerably among forecast centers and over time. Forecast centers use any of the following data source when available: in situ observations (e.g., ships, buoys, station reports, aircraft reports), remotely sensed data (e.g., active and passive sensors on aircraft and satellite platforms) and data scenes, and TC-specific applications (e.g., algorithms that prescribe circulations based on intensity, forward speed, patterns in satellite images, etc.)—these are discussed in detail in Section 3. Section 4 documents historical records of objective wind structure estimates used for best track datasets, followed by needs in both the operational and research communities. We provide recommendations for addressing operational needs in future sensor development. Finally, Section 5 summarizes the review and discusses potential solutions in development.

2. Operational center estimates of TC surface winds

Surface winds from operational centers include quantities like RMW, R64, R50, and R34 to represent the wind field. While operational centers issue advisories with wind radii, the wind-averaging criteria vary across the agencies (U.S. warning centers use a 1-min sustained wind speed while many other forecasting centers use 10-min averages). And, despite VMAX, TC location, and movement being common to all advisories, TC wind structure specification differs. For example, U.S. TC warning centers, namely the National Hurricane Center (NHC), the Central Pacific Hurricane Center (CPHC), and the Joint Typhoon Warning Center (JTWC), provide estimates of R64, R50, and R34 in geographic quadrants surrounding the storm. These centers estimate RMW and include those parameters in numerical model input files (i.e., "TC vitals" files – described later) but not in current advisories. The WMO Regional Specialized Meteorological Centre (RSMC) in La Reunion and the TC warning centers in Australia also analyze the wind radii at the same threshold intensities. But, RSMC Nadi analyzes the radius of 33-kt, 47-kt and 64-kt winds, RSMC New Delhi analyzes 28-kt winds in addition to R64, R50 and R34 (India Meteorological Department, 2021), and RMSC Tokyo analyzes both 30-kt winds (R30) and R50.

Although wind radii estimates are mandatory in advisories, aircraft reconnaissance and surface observations were the only data sources available to analyze the wind in the pre-satellite era (early 1970s). For instance, NHC started forecasting 24-h R50 in 1958, and added forecasts of 24-h R34 in 1979; 36-h R34 and R50 in 1988; R64 to 36 h in 1995 and to 48 h in 2018; and R34 and R50 to 72 h in 2001 (NHC, 2019). JTWC similarly estimated and forecasted varying wind speed thresholds through the years (JTWC, 1975; JTWC, 1992; JTWC, 2004; JTWC, 2019). Since 2016, JTWC's wind radii forecasts for R34, R50, and R64 have extended through the entire 120-h forecast period (JTWC, 2016). Fig. 1 indicates these real-time wind radii estimates as black lines.

Operational centers also analyze a variety of vortex parameters in near real-time to generate a "bogus vortex," defined as "a representation of a tropical vortex based on a blend of observed surface winds and typical tropical storm wind profiles" (AMS Glossary of Meteorology, 2020; Holland, 1993). This "bogus vortex"—sometimes referred to as the "TC bogus" or "bogus" in older tropical cyclone reports—is transmitted by operational centers for assimilation by certain global and regional modeling systems. Operationally-generated vortex parameter files may include storm identifier, date, time (current and past times), TC location, intensity, central pressure, storm type, wind radii, the pressure and radius of the outermost closed isobar (ROCI), RMW, eye diameter, geographical sub-region, maximum seas, storm motion, system depth, and wave heights.

Operational centers also maintain those vortex parameters records in various formats. For example, records at JTWC, NHC, and CPHC are stored in Combined Automated Request Query (CARQ) lines in the Automated Tropical Cyclone Forecast (ATCF; Miller et al., 1990; Sampson and Schrader, 2000) files or "adecks." Often, the post-season best tracks retain these operationally-estimated vortex parameters (Knapp et al., 2010; Landsea and Franklin, 2013; Bureau of

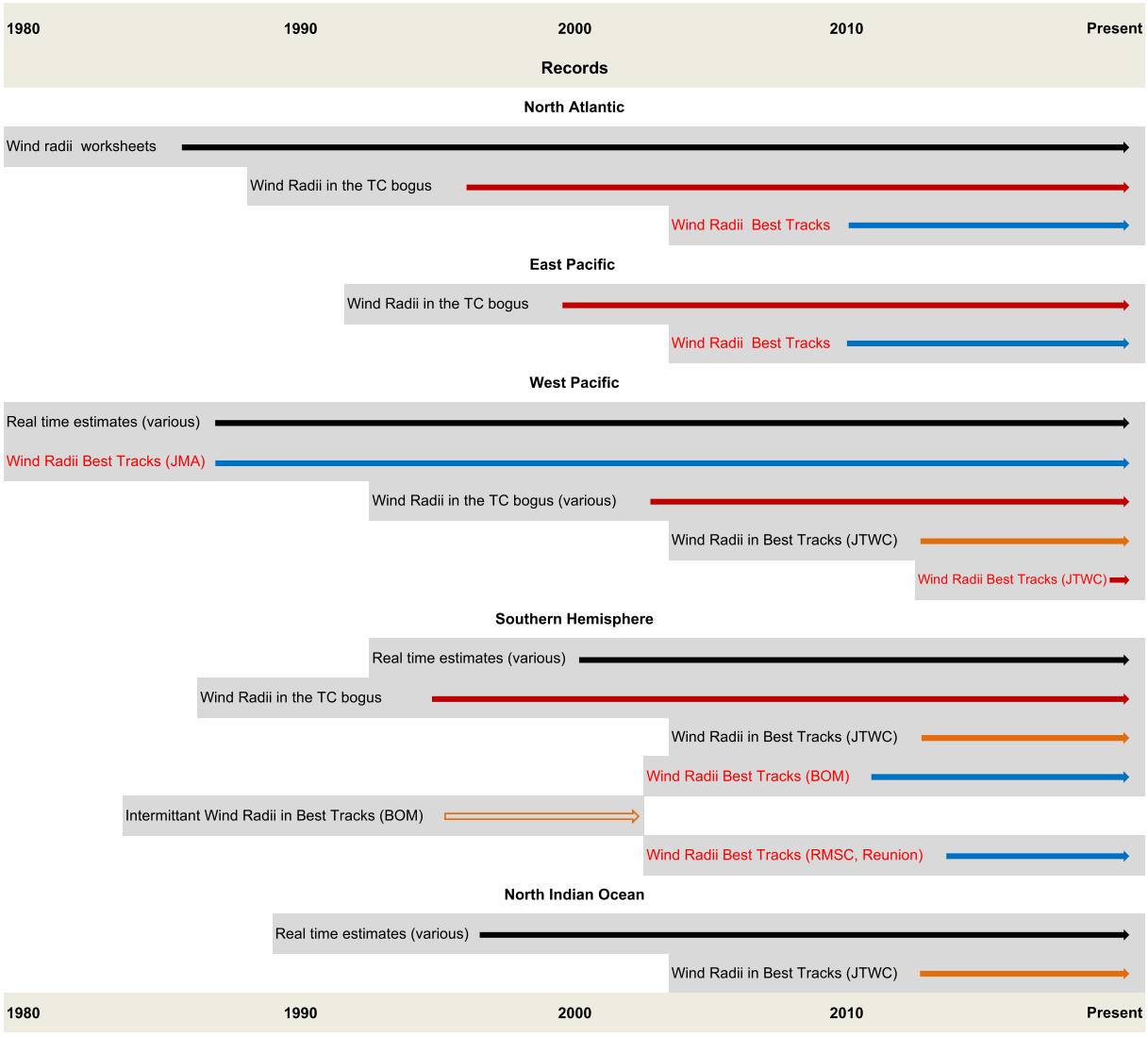

Fig. 1. Records of TC surface wind/wind radii since 1980 by TC basin. Black bars indicate paper records, red bars indicate digital records of operationally created estimates, orange bars indicate wind radii are in best tracks, but they have not yet been reanalyzed, and blue bars indicate best track values that have been reanalyzed in the post-season. Gray horizontal areas (including text and arrows) indicate the time periods during which annotated information was available. Red text indicates best tracks that contain post-storm reanalyzed wind radii information.

Meteorology, 2020; JMA, 2020) as shown in Fig. 1 by red horizontal lines. While in the best tracks, parameters like ROCI and RMW[1] are not subjected to vigorous post-storm review. In older best track archives, only location and intensity have undergone post-storm review. Orange horizontal lines in Fig. 1 indicate the years when non-reviewed wind radii are present in the best track archives. North Atlantic and eastern North Pacific basin paper records of R34, R50, and R64 extend back into the 1980s (Fig. 1), but post-storm analysis only began in 2004 (HURDAT2; Landsea and Franklin, 2013). Post-storm analyzed wind radii records are indicated by blue horizontal lines in Fig. 1.

The time periods and parameters included in operational center best track records vary. To address this, the Extended Best Track Dataset (Demuth et al., 2006), used extensively by the research community, provides an amalgam of best track position and intensity with RMW, R34, R50, and R64 (pre-2004) in NHC's area of responsibility from the 1980s onward. JTWC best tracks include wind radii starting in the early 2000s, but post-storm analysis of R34 for western North Pacific tropical cyclones, and coincident regression of R50 and R64 estimates based on R34, only began in 2016 (Sampson et al., 2017)—indicated by a blue line in Fig. 1. RSMC Tokyo maintains the longest best track record of TC surface wind structure, which includes the longest and shortest axis of R30 and R50 in geographic octants around western North Pacific tropical cyclones from 1979 onward (JMA, 2020). The Australian Bureau of Meteorology also maintains a best-track database that includes wind radii for tropical cyclones in its

[1] Starting with the 2021 hurricane season, NHC will provide post-storm best track values of RMW for the North Atlantic and Eastern North Pacific basins (Christopher Landsea, Personal Communication, 2021).

area of responsibility (Bureau of Meteorology, 2020). Also, they have recorded wind radii in best track data archives since the 2003–2004 season, though operational estimates exist intermittently back to 1983. Finally, RSMC La Reunion maintains a best track database for the South Indian Ocean that includes radii data from the 2003–2004 season onward. Other RSMCs do not provide wind radii in their best track data archives (Knapp et al., 2018).

Finally, since analysis of surface winds can be a time-consuming process, quality and consistency of estimates also depend on staffing and staffing priorities. The centers that created the best track file are a good source for such information.

3. Objective estimates of TC surface winds

Since the estimates are from disparate data sources, forecasters have a great deal to interpret when applying these estimates to their TC surface wind best tracking process. This section discusses the objective estimates used to construct the subjective best track datasets described. And, to assist with the process, this section also discusses wind sampling and averaging considerations, outlines objective methods, relevant archives, and finishes with a summary section with a figure intended for use as a quick reference in operations.

3.1. Sampling and averaging considerations

Each sensor (e.g., an anemometer at a fixed location, a falling dropwindsonde, or an instantaneous measurement of radiance) can yield markedly different wind speed values for the same location and time, and sampling period, observation level, and averaging partly explain those differences. There are many studies of aircraft data, so we use them to highlight the issues.

Franklin et al. (2003) used mean dropwindsonde (Hock and Franklin, 1999) profiles at two levels to determine relationships that convert winds at one level to winds at another. Others (e.g., Uhlhorn et al., 2007; Klotz and Uhlhorn, 2014; Sapp et al., 2019) developed the Stepped Frequency Microwave Radiometer (SFMR) wind speed retrievals (details in section 3b) to estimate 10-m winds in the hurricane environment. These SFMR retrievals are based on relationships identified in mean dropwindsonde profiles. While the aircraft and dropwindsonde are moving independently in space, a 10-s average SFMR wind observation is trained to the characteristic dropwindsonde surface. SFMR relationships are empirical and have gone through various revisions as data improves. Recently, NHC noticed a discrepancy between SFMR wind speeds and surface winds estimated from flight-level observations on the aircraft, particularly in TCs with intensities above 115 kt (60 m s^{-1}) in 2017 and following years. Investigation with a larger dropwindsonde-based near surface winds database shows high biases of 1 kt, 5 kt, 7 kt, and 10 kt at 80 kt, 120 kt, 140 kt, and 165 kt surface winds, respectively (Heather Holbach, Personal Communication, 2021). Further complicating the problem, SFMR typically underestimates wind maxima by about 10% due to under-sampling (Uhlhorn and Nolan, 2012; Klotz and Nolan, 2019). Despite recalibration and under-sampling issues, dropwindsonde data and SFMR observations are considered to be the most accurate observations of wind within a TC and are used to train and validate other algorithms.

3.2. Operationally-available data (latency <4 h)

As stated earlier, observations delivered to forecasters within 4 h are considered operationally available. These include aircraft-based SFMR, low Earth orbiting satellite-based radiometers Advanced Microwave Scanning Radiometer-2 (AMSR2), Soil Moisture Active Passive (SMAP), Soil Moisture Ocean Salinity (SMOS), and space-borne active radars including the Advance Scatterometer (ASCAT), HY-2 scatterometers (HSCAT), and Scatterometer Satellite (SCATSAT).

3.2.1. Aircraft reconnaissance

Aircraft reconnaissance has provided decades of data for select storms (Guard et al., 1992; Williams, 2015). Prior to upgraded instrumentation on reconnaissance aircraft in the late 1970's (NOAA's research aircraft) and early 1990's (U.S. Air Force Aircraft), accurate flight-level winds were unavailable. For historical insight on aircraft observations, see Sheets, (1990), Guard et al. (1992), Rappaport et al. (2009), Hagen and Landsea (2012), and Landsea and Franklin (2013). Today's aircraft reconnaissance employs high-quality navigation and instrumentation (OMAO, 2020) and provides flight-level wind data for operational reconnaissance use (OFCM, 2019). NHC formalized methods to estimate surface winds from flight level by 2000 (Franklin et al., 2003; Rappaport et al., 2009). Operational flight levels are 5000 feet (1500 m) and 10,000 feet (3000 m) for tropical storms and hurricanes, respectively. Research aircraft make similar observations, but their altitude varies depending on mission priorities. Most operational aircraft reconnaissance is flown in the North Atlantic with occasional operational missions in the eastern and central North Pacific (OFCM, 2019). U.S. operational and research low-level reconnaissance missions produce flight-level observations that analysts use to infer surface winds (e.g., Franklin et al., 2003). Most operational missions deploy Global Positioning System (GPS) dropwindsondes (Hock and Franklin, 1999) to measure the environment from the flight level to the ocean surface. In addition, NOAA and U.S. Air Force planes carry a SFMR sensor (Jones et al., 1981; Black et al., 1995; Uhlhorn and Black, 2003; Uhlhorn et al., 2007; Klotz and Uhlhorn, 2014), which provides surface wind speeds and rainfall rates along the aircraft path. Approximately 30% of the Atlantic TC life times are observed via aircraft (Rappaport et al., 2009). Research missions occur in other basins. (e.g., Wu et al., 2005; Elsberry and Harr, 2008; T-PARC 2008), and recently several countries (i.e., China, Korea, India, Taiwan, and Japan) have initiated aircraft reconnaissance (e.g., Chan et al., 2011; Wong et al., 2014; Reade, 2014; Yamada et al., 2018). Most flights outside the

Atlantic are intermittent and some of the aircraft cannot penetrate the TC core. Although aircraft observations are extensively used when available, there is a heavy reliance on satellite reconnaissance of TCs in all basins.

3.2.2. Microwave radiometers

Microwave instruments are either passive (receive only) or active (transmitting and receiving), and their applicability to retrieving wind observations depends on the frequency. Microwave frequencies (300 MHz–300 GHz) and wavelengths (1 m–1 mm) have several atmospheric windows that are useful for many atmospheric applications and complement traditional visible and infrared frequencies associated with geostationary satellites. Since meteorological microwave frequencies are often described in terms of bands, see Table 2 for this information. Radiative transmissivity at most frequencies within the microwave spectrum is minimally and selectively affected by cloud particles and smoke, and observations in microwave bands are not degraded by reflection of sunlight off the Earth's surface. However, the microwave energy emitted by the Earth is small relative to reflectance and decreases with increasing wavelength, so microwave instruments require large receivers (dishes) with high signal sensitivity. These low Earth orbiting microwave instruments have large Earth surface footprints and low spatial resolution due to their longer wavelengths.

The high transmissivity of most microwave radiation through Earth's atmosphere and the relationship between wind speed and ocean surface emissivity at longer C-band and L-band microwave wavelengths allows scientists to estimate the extreme wind speeds associated with TCs over the open ocean using microwave sensor observations. Emissions from wind-roughened ocean surface also increase nearly linearly with wind speed at these longer wavelengths (Nordberg et al., 1971; Monahan and O'Muircheartaigh, 1980; Reul and Chapron, 2003; Anguelova and Webster, 2006, Hwang et al., 2019a, 2019b). The C-band signal (4–8 GHz; 7.5–3.75 cm) does not saturate in extreme winds, even up to 135 kt (70 m s-1) and above (Reul et al., 2012, 2016; Yueh et al., 2013; Meissner et al., 2014, 2017; Fore et al., 2016). However, C-Band signals attenuate in extreme rainfall (Tournadre and Quilfen, 2003; Alpers et al., 2016), which often occurs in TCs.

Table 2
Microwave band codes typically used in meteorological applications.

Band	Wavelength [cm]	Frequency [GHz]
mm	0.1–0.27	300–110
W	0.27–0.4	110–75
V	0.4–0.75	75–40
Ka	0.75–1.11	40–27
K	1.11–1.67	27–18
Ku	1.67–2.4	18.0–12.5
X	2.4–3.8	12.5–8.0
C	3.9–7.5	8.0–4.0
S	7.5–15.0	4.0–2.0
L	15.0–30.0	2.0–1.0

3.2.3. SFMR

SFMR, a passive C-band instrument, senses microwave radiation from six frequencies emitted by the ocean surface. Wind speed estimates and rain rate estimates are retrieved simultaneously using the six channels that are sensitive to ocean roughness and wind speed. Precipitation is an absorber at these frequencies and the absorption has a stronger dependence on frequency in the presence of rain. Using this characteristic over narrowly spaced frequencies, the SFMR algorithm estimates both the wind speed and rain rate. Over the years, extensive calibration efforts have improved SFMR wind speed estimates (Uhlhorn and Black, 2003; Uhlhorn et al., 2007; Klotz and Uhlhorn, 2014; Sapp et al., 2019), which are still ongoing as discussed in section 2. SFMR observations are often considered the best ground truth for satellite-based sensors (Sapp et al., 2019) with sensitivity to wind speeds from 30 kt (15 m s^{-1}) to 150 kt (75 m s^{-1}) and errors of 6–14 kt (3–7 m s^{-1}), as seen in Table 3. Standardization of inherently pointwise and instantaneous SFMR data is required to account for spatial and temporal averaging differences.

3.2.4. Space-based radiometers

Unlike higher-frequency radiometers, L-band (1–2 GHz; 30–15 cm) radiometers are mostly unaffected by liquid or frozen precipitation (Wentz, 2005; Reul et al., 2012). For wind speeds below 30 kt (15 m s^{-1}), the performance of L-band radiometers is typically poor relative to other sensors. This performance issue is due to larger radiometer noise and lower sensitivity of the L-band radiometers. However, L-band radiometers provide measurements of extreme ocean wind speeds up to 150 kt (75 m s^{-1}) (Reul et al., 2016, 2017; Yueh et al., 2016; Meissner et al., 2017). The 40- to 60-km resolution of current L-band radiometers prohibit observation of small scale features such as eyewalls, and likely underestimate extreme wind speeds in these regions. L-band wind speed retrievals also require ancillary ocean surface temperature and salinity from an ocean model like the Hybrid Coordinate Ocean Model (Metzger et al., 2008). Thus, wind speed estimates are typically too high in areas such as the mouth of the Amazon where salinity is low and poorly resolved in daily model analyses. L-band wind retrievals may also be adversely affected by radio/cell phone interference (Soldo et al., 2015; Mohammed et al., 2016).

Other passive observing systems (Table 3) that currently enable low-latency surface wind speed estimates inside the rainy TC environment include the AMSR2 (Tachi et al., 1989; Kawanishi and coauthors, 2003; Imaoka et al., 2010), SMAP (Entekhabi et al., 2004), and SMOS (Mecklenburg et al., 2016). The WindSat sensor (Gaiser et al., 2004) provided microwave observations for TCs until May 2021; data from that sensor for past TCs are available in archives (see the data availability statement). For each of these observing systems there is at least one algorithm that provides all-weather surface wind estimates, each trained on and/or tested against SFMR data. As evident in Table 3, each observing system has its own frequency (or frequencies), swath width, and surface footprint

Table 3
Summary of remote sensing wind speed/vector estimation methods discussed in Section 3. Wind speeds are expressed in operational units of kt (1 kt = 0.514 ms^{-1}). The term "VMAX support" implies such data may, at times, provide information relevant, particularly a minimum, for the operational estimation of VMAX. Large RMW are defined here as greater than 75 km or the 75th percentile following Kimball and Mulekar (2004).

Name	Type of data	Channels	Swath width	Data footprint size	TC Wind speed Ranges (kt)	Errors (kt)	Caveats	Suggested Use	References
SFMR	Wind speed	6 Channels ranging from 4.6 to 7.2 GHz	22° beam width	30s sample: At 0.3 km 0.2 × 3.9 km At 1.5 km 0.6 × 5.1 km At 3 km 1.3 × 7.2 km	30−150	6−14	• Availability (aircraft only) • Errors are largest in rain <50 kt • An increasing high biased above 80 kt (10 kt @ 165 kt) • Limited Spatial coverage	Ground Truth RMW VMAX R34 R50 R64	Sapp et al. (2019) Uhlhorn and Black (2003) Uhlhorn et al. (2007) Klotz and Uhlhorn (2014)
AMSR2	Wind speed	6.9 GHz 10.7 GHz 18.7 GHz 23.8 GHz 36.6 GHz 89.0 GHz	1450 km	25 × 25 km	0−60 (NESDIS) 0-140 (JAXA)	? 14	• Not available within 50 km of land • Flagged errors can be caused by sun glint and radio interference	Large RMW VMAX support R34 R50 R64	Alsweiss et al. (2018) Shibata (2006) Shibata (2002) Chang et al. (2015)
ASCAT	Wind vectors	5.3 GHz	two 550 km wide swaths	25 km (common) 12.5 km (hi-resolution/coastal)	0−70	3	• Saturation starts near 50 kt • Wind speeds saturate near 70 kt	Large RMW VMAX support R34 R50	Verspeek et al. (2010) Ricciardulli and Wentz (2015) Soisuvarn et al. (2013) Stoffelen et al., 2017
OSCAT	Wind vectors	13.5 GHz	1800 km	25 km 50 km	0−60	3	• Saturation starts near 50 kt • Wind speeds saturate near 70 kt • Sensitive to heavy rainfall (rain flagged) • Noisier than C-band in TC environment	Large RMWs R34 R50	Gohil et al. (2013) Lin et al. (2018)
HY-2B/C	Wind vectors	13.25 GHz	1800 km	25 km	0−60		• Saturation starts near 50 kt • Wind speeds saturate near 70 kt • Sensitive to heavy rainfall (rain flagged) • Noisier than C-band in TC environment	Large RMWs R34 R50	Wang et al. (2020) Zhao et al. (2016) Zhao and Zhao (2019)

(*continued on next page*)

Table 3 (*continued*)

Name	Type of data	Channels	Swath width	Data footprint size	TC Wind speed Ranges (kt)	Errors (kt)	Caveats	Suggested Use	References
SMAP	Wind speed	1.4 GHz	1000 km	40 km RSS 60 km JPL	25–150	4–9	• Requires ancillary sea surface temperature and salinity • Large error possible in areas of fresh water intrusion like river deltas.	VMAX support VMAX support R34 R50 R64	Meissner et al. (2014) Yueh et al. (2016) Meissner et al. (2017) Fore et al. (2018)
SMOS	Wind speed	1.4 GHz	1000 km	40 km	15–75	5–7	• Requires ancillary sea surface temperature and salinity • Large error possible in areas of fresh water intrusion like river deltas.	VMAX support R34 R50 R64	Reul et al. (2012) Yueh et al. (2013) Reul et al. (2016) Yueh et al. (2016) Meissner et al. (2017)
SAR	Wind speed	5.4 GHz	400 km in Extra Wide Swath Mode	20 × 40 m	0–150	5	• Intermittent nature of acquisitions • Can be more latent • Spatial averaging (3 × 3 km) used to approximate 1-min sustained winds • Some attenuation in extreme (>80 mm) precipitation	RMW VMAX R34 R50 R64	Zhang et al. (2012) Horstmann et al. (2015) Hwang et al. (2015) Mouche et al. (2017) Mouche et al. (2019)
WindSat (all-weather)	Wind Speed	6.9 GHz 10.7 GHz 18.7 GHz 23.8 GHz 36.6 GHz	1025 km	25 × 35 km	0–150	4–8	• Not available within 50 km of Land	Large RMW VMAX support R34 R50 R64	Meissner et al. (2021) Manaster et al. (2021)
CYGNSS	Wind Speed	1.6 GHz	Along reflection points	15 × 15 km	10–70	2–12	• Sensitive to variability of GPS/GNSS transmission signals • Coverage is limited • Errors increase with wind speed • Dependent on sea state (fully developed vs. young seas), latter typical in TCs	VMAX support R34* R50* R64*	Ruf and Balasubramaniam (2018) Ruf et al. (2018) Ruf et al. (2019) Morris and Ruf (2017a), b

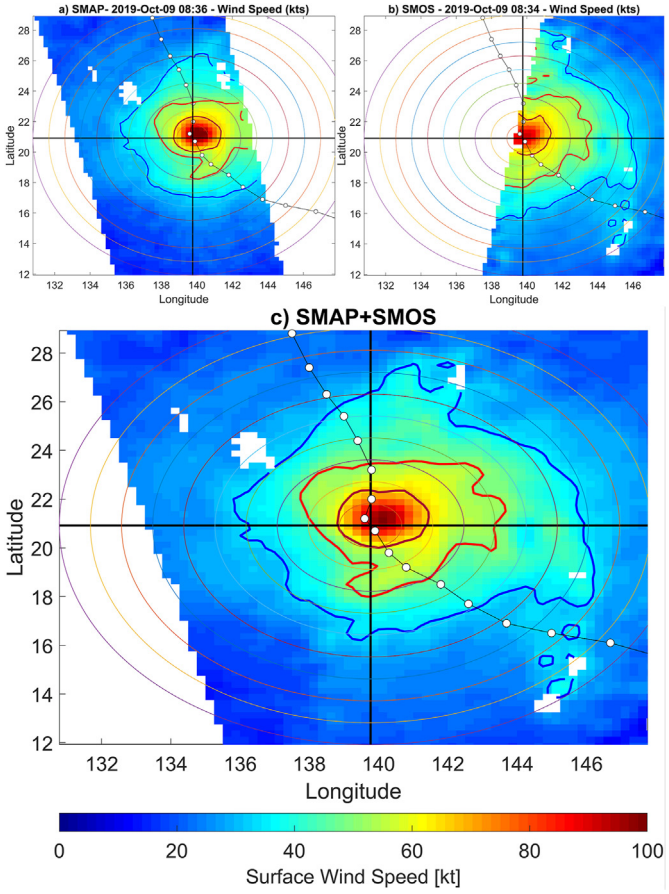

Fig. 2. Surface wind speed retrieved from (top left) SMAP and (top right) SMOS as the satellite swaths covered Typhoon Hagibis on November 9, 2019 at 0836 UTC and 0834 UTC, respectively. c) Merged SMOS + SMAP surface wind field. Wind speed contours at 34-kt (thick blue curve), 50-kt (red thick curve) and 64-kt (magenta curve) are superimposed with the background wind fields. The thin color circles indicate radii from TC center to 1000 km in 100-km increments.

characteristics. Accordingly, each observing system can observe a different wind speed range and has unique error characteristics. Table 3 includes caveats, suggested uses, and related references for each system. In this section, we summarize the primary characteristics of each observing system that are relevant to practical application in TC forecasting, using Table 3 as our guide.

3.2.5. AMSR2

AMSR2 is a conical scanner that detects frequencies within bands centered at 6.9, 10.65, 18.7, 23.8, 36.6 and 89.0 GHz, and has vertical and horizontal polarization. Each AMSR2 channel is sensitive to surface winds, but individual bands are attenuated to varying degrees by cloud water (increased attenuation with increased frequency), water vapor (peak near 20 GHz), SST (peak near 7 GHz), and ice. WindSat includes the same channels, except 89 GHz. Wind retrieval from both sensors follow the same process as SFMR, using multiple channels and eliminating signals related to SST changes, cloud water, and precipitation. There are multiple AMSR2 wind speed algorithms (Alsweiss et al., 2018; Chang et al., 2015; Meissner and Wentz, 2009; Shibata, 2002, 2006; Zabolotskikh et al., 2015), two of which are available in operations: NOAA's Center for Satellite Applications and Research (Chang et al., 2015; Alsweiss et al., 2018) and the Japan Aerospace Exploration Agency's (JAXA) all-weather Sea Surface Wind Speed algorithm (Shibata, 2002, 2006). Each algorithm provides wind speed estimates at a resolution of 25 km. The JAXA algorithm is trained using buoy data, and the NOAA algorithm is trained using buoy and SFMR data gathered in tropical and extra-tropical cyclones. AMSR2 winds are flagged in areas of sun glint and radio interference. An inter-comparison of these products (Alsweiss et al., 2018) suggests that both are applicable for TC operations for wind speeds up to 140 kt (70 m s^{-1}), although the reported applicability ranges are product dependent as are reported errors, which could be as high as 14 kt (7m s^{-1}). AMSR2 wind speed are available from JAXA, NOAA, and Remote Sensing Systems. Existing WindSat algorithms (e.g., Bettenhausen et al., 2006) that provide wind vectors have generally performed poorly in TCs, but new WindSat all-weather wind speed algorithms, discussed in section 3.3, show more promise (Meissner et al., 2021). At this time, AMSR2 wind speeds are available to NHC and JTWC, but NHC is not using these in operations.

3.2.6. SMAP and SMOS

NASA's SMAP Mission/Satellite (Entekhabi et al., 2010, 2014) was designed to provide soil moisture and freeze/thaw information using passive L-band (1.4 GHz) radiometer and active L-band (1.2 GHz) radar instruments that share a 6-m dish. The radar on SMAP failed in July 2015, but the radiometer continues to operate. SMAP brightness temperatures retrievals over oceans are also available to estimate wind speed. Two algorithms are presented in Meissner et al. (2014; 2017), which produces a 40 km resolution product, and in Fore et al. (2018) and Yueh et al. (2016), which produces a 60 km resolution product (Table 3). Meissner et al. (2017) and Fore et al. (2018) used SFMR averaged over matching 25 km and 60 km SMAP resolutions for training, respectively. The use of smaller averaging areas leads to higher wind speed estimates from the Meissner et al. (2017) product. Wind speed estimates from both algorithms are available in near real-time. The NASA/JPL product (Fore et al., 2018) and the Remote Sensing Systems product (Meissner et al., 2017) are accessible from sites listed in the data availability statement. SMAP wind speeds are useful in the range 25–150 kt (12–75 m s^{-1}) with errors of 3.5–9 kt (1.8–4.5 m s^{-1}). However, the effective extreme wind speeds are limited by sensor resolution and the algorithms' training methods. Fig. 2a shows an example of Meissner et al. (2017) SMAP wind speed estimates for Typhoon Hagibis, including R34, R50, and R64 estimates, on October 9, 2019 at 0800 UTC. At this time, JTWC estimated intensity around 140 kt, while the 40-km pixel sized SMAP/SMOS composite indicated extremes of just over 100 kt.

The European Space Agency (ESA) Soil Moisture and Ocean Salinity (SMOS; Kerr et al., 2010; Mecklenburg et al., 2016) is a synthetic aperture radiometer that measures the

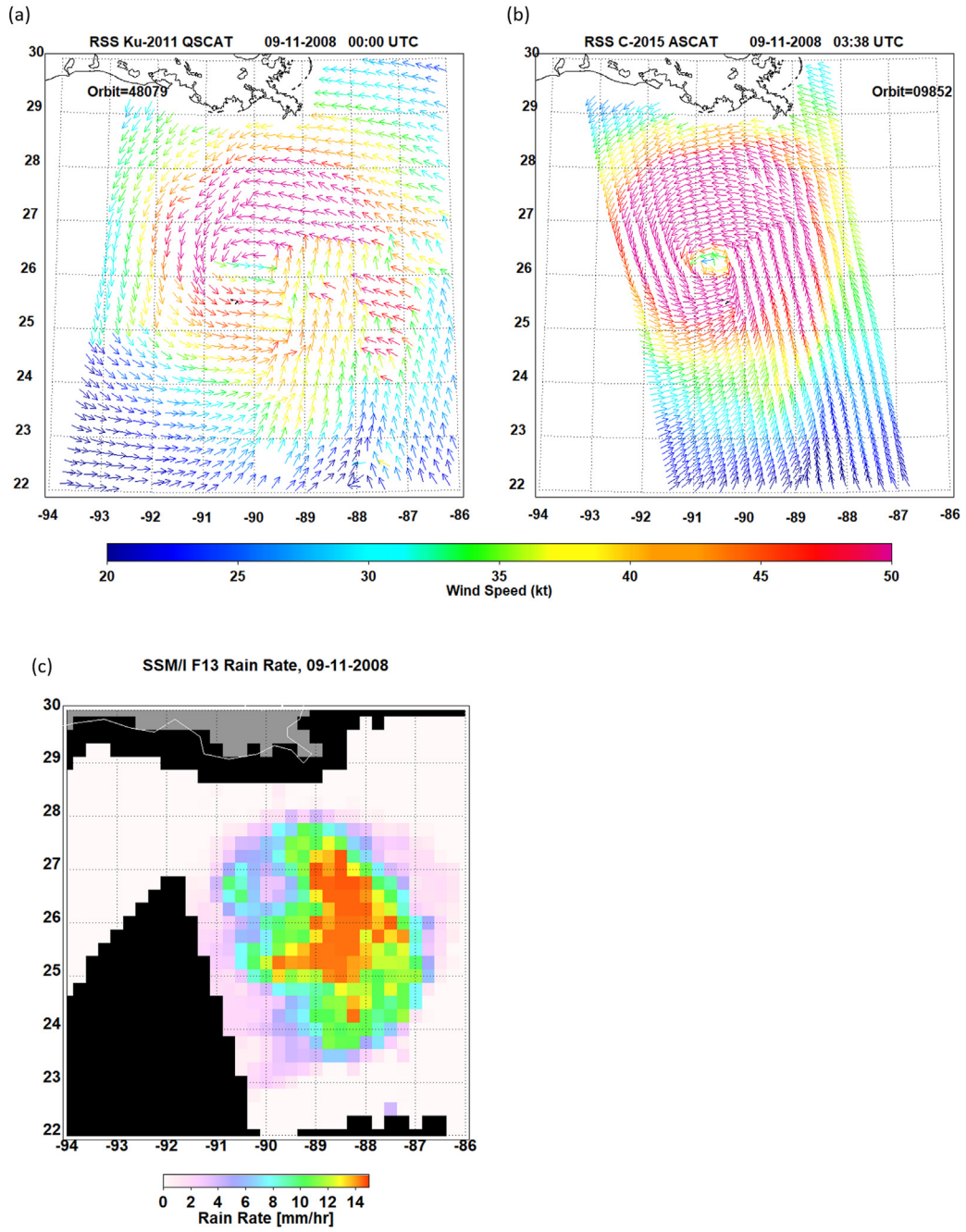

Fig. 3. (top left) Wind vector in Hurricane Ike, on September 11, 2008, QuikSCAT and (top right) ASCAT-A and rain rate from Special Sensor Microwave Imager (SSM/I) (bottom left). The QuikSCAT wind field is rain contaminated, as indicated by a negative bias in depicted wind speeds (southeast quadrant) and wind vectors rotated perpendicular to the satellite track. ASCAT is mostly unaffected by rain at these wind speeds and rain intensity.

spatial Fourier transform of the emitted brightness temperature, which is referred to as *visibility*. This *visibility* function is converted into scene brightness temperatures, from which the surface wind speed can be retrieved. SMOS data were trained using a combination of SFMR and the Hurricane Research Division's H*Wind (Powell et al., 1998, section 3c) analyses. Training data sampled within 12 h of each SMOS observation were averaged using 2D Gaussian windows with a standard deviation of 43 km, and the resultant averages were extrapolated to match SMOS sensor resolution. The details about retrieving winds speeds based on SFMR filtered averages and their validation are provided by Reul et al. (2012, 2016, 2017) and Yueh et al. (2013). Near real-time data access is available from ESA in the form of SMOS-based wind speeds and Automated Tropical Cyclone Forecast System (ATCF; Sampson and Schrader, 2000) formatted "fixes" (estimates of intensity and wind radii in text form). SMOS wind speeds are applicable in the range 30–150 kt (15–75 m s^{-1}) with errors of 5.4–7.2 kt (2.7–3.6 m s^{-1}). Fig. 2b shows a SMOS surface wind speed analysis for Hagibis, and Fig. 2c combines both

Table 4
Summary of satellite applications designed to estimate tropical cyclone operational wind structure metrics. Shown are the name of the method, the satellite channels utilized, the effective resolution of metric estimation, estimated mean errors, caveats, suggested uses, and references. Here we use operational units of n mi (1 n mi = 1.852 km).

Name	Channels	Output Resolution (n mi)	Mean Errors (n mi)	Caveats	Suggested Use	References
IR-vortex	~11.0 μm	5	25	• Requires current location, motion and intensity information • Works best for mature symmetric TCs	R34 R50 R64	Knaff et al. (2016)
Microwave Sounders	50 GHz	5	30	• Requires current location, motion and intensity information for wind radii • Performs poorly in small TCs	VMAX support (in weak TCs) R34 R50 R64	Demuth et al. (2006)
Multi-Platform Estimates	N/A	10	30	• Requires current location, motion and intensity information • Estimates are too low for very large TCs	RMW R34 R50 R64	Knaff et al. (2011)

SMAP and SMOS wind speed analyses on the same image as they are nearly concurrent passes. The concurrent passes not only indicate a more complete depiction of the wind speed structure; they demonstrate some consistency between the two L-Band swaths.

3.2.7. Scatterometers

Scatterometers (Table 3) are primary sources of surface winds for TC forecast operations (Brennan et al., 2009)—ASCAT remains a critical asset at NHC and JTWC even today. They have the longest history of any satellite-based surface wind observation sensor, starting in 1991 with the European Remote Sensing (ERS-1 and ERS-2) C-band scatterometers (Attema, 1991; Stoffelen, 1998). Numerous scatterometers have launched since then, including NASA's much-cited Ku-band scatterometer, QuikScat (Lungu and Callahan, 2006), in 1999. While scatterometer data are most applicable for estimating R34, the sensors provide trustworthy wind speed measurements up to around 65 kt (33 m s^{-1}), with mean errors around 3 kt (1.5 m s^{-1}). Wind speed detection has decreased sensitivity starting at 50 kt (25 m s^{-1}) with complete signal saturation at approximately 70 kt (35 m s^{-1}) (Wentz and Smith, 1999; Verspeek et al., 2010; Ricciardulli and Wentz, 2015; Soisuvarn et al., 2013; Stoffelen et al., 2017a). Errors can be much larger in strong wind speed gradients such as those near the RMW due to the coarse spatial resolution. Despite the typical signal saturation, ASCAT has produced winds of 85 kt in very strong extratropical cyclones (see https://storymaps.arcgis.com/stories/83038d799d7249b68e81be1aa7ff84fd).

Three operationally available scatterometer types used frequently for near real-time TC observation are the Advanced Scatterometer (ASCAT; Figa-Saldaña et al., 2002), SCATSAT[2] (Misra et al., 2019), and the HY-2 scatterometer (HSCAT) (Zhao et al., 2016). ASCAT, HSCAT and SCATSAT operate in a co-polarized manner where the radar signal is emitted and received in the same polarization. ASCAT is a C-band scatterometer (5.225 GHz) carried onboard three operational satellites, Europe's Meteorological Operational satellite (Metop)-A, -B, and −C. SCATSAT and its shared-design predecessor, OSCAT, carried on the Indian OceanSat satellite are Ku-band scatterometers with larger swatch widths (Table 3). Ku-band wind retrievals are impacted by rainfall in TCs (Stiles and Yueh, 2002; Tournadre and Quilfen, 2003; Draper and Long, 2004; Hilburn et al., 2006; Weissman and Bourassa, 2008; Portabella et al., 2012). The Ku-band also starts losing sensitivity at about 50 kt (25 m s^{-1}) with complete loss above 60 kt (30 m s^{-1}). Much like SCATSAT, HSCAT is a scatterometer operating in Ku-band at 13.25 GHz which traces out a ~1300 km, and as such suffer from the same impacts from rainfall and saturation near 50 kt (25 m s^{-1}), and has performance similar to SCATSAT (Zhao and Zhao, 2019; Wang et al., 2020; Ad

[2] discontinued following an irrecoverable instrument failure on 28 February 2021.

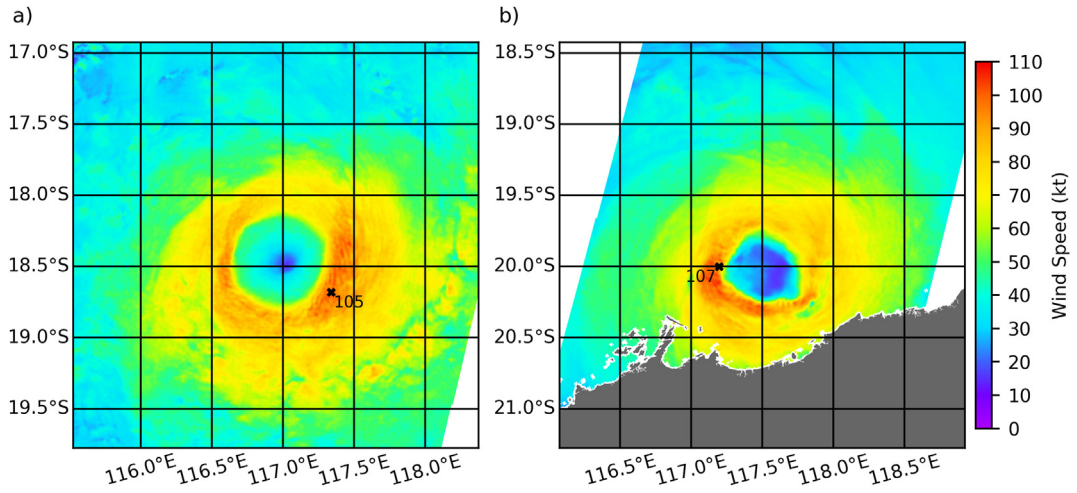

Fig. 4. SAR wind speed estimates for Tropical Cyclone Veronica (2019) as it approached Western Australia (a) valid March 22, 2019 at 2147 UTC and (b) valid March 23, 2019 at 2139 UTC. Black x's mark the location of the maximum winds and provide the wind speed in units of kt. JTWC's best track data indicate that the storm intensity was 95–110 kt on the 22nd and 85–105 kt on the 23rd.

Stoffelen, personal communication 2021). It is notable that HY-2C is not in a sun synchronous orbit that will allow more regular comparisons to other satellite-bases estimates. ASCAT SCATSAT, and HSCAT data are available from the Koninklijk Nederlands Meteorologisch Institute (KMNI) based on their algorithms. Usage of these data varies. For example, JTWC using all of the above mentioned scatterometer data while NHC only uses ASCAT routinely.

Several algorithms based on empirical models, known as Geophysical Model Functions (GMFs), have been developed to estimate surface wind vectors from ASCAT (Wentz and Smith, 1999; Verspeek et al., 2010; Ricciardulli and Wentz, 2015; Soisuvarn et al., 2013; Stoffelen et al., 2017a) and SCATSAT and HSCAT (Gohil et al., 2013; Lin et al., 2018) data. Most ASCAT algorithms used in operations are produce 25 km resolution products, but coastal or high-resolution ASCAT is available from KNMI and Brigham Young University. Scatterometer wind retrieval algorithms are primarily trained using buoy data. The impact of rain on wind retrievals is dependent on the sensor wavelength, as illustrated in Fig. 3. The C-band (ASCAT) wind speeds are much higher and less attenuated than those from a Ku-band instrument (Fig. 3a and b), and wind directions in the C-band remain cyclone-like in the rainy area shown by the Special Sensor Microwave Imager/Sounder (SSMIS) rain rates in Fig. 3c.

3.2.8. Indirect measurements

Operational forecast centers and supporting organizations also use a variety of techniques to generate wind radii wind estimates from infrared (IR) imagery, microwave sounders, and multi-platform technique inputs including scatterometers, infrared imagery, and microwave sounders (Table 4). Infrared wind radii estimates are based on empirical relationships between the size of the IR cloud shield and the size and intensity of a TC (JTWC, 1989,1990; Rupp and Lander, 1996). These relationships have been formalized in many studies (Dolling et al., 2016; Knaff et al., 2014, 2016; Kossin et al., 2007; Lee et al., 2010; Piñeros et al., 2008, 2010; Reul et al., 2016). The Knaff et al., (2016) method uses a modified Rankine vortex (Depperman, 1947) to provide wind radii for subjective (Dvorak, 1984; Velden et al., 2006) and objective Dvorak intensity estimates (Olander and Velden, 2019). Another algorithm uses data from microwave sounders aboard several operational satellites [NOAA-18, -19, −20, Metop-A, -B, −C, Suomi National Polar-orbiting Partnership (SNPP)] to derive both VMAX and wind radii (Demuth et al., 2006). Yet another, multi-platform algorithm analyzes information from IR images (Knaff et al., 2015), microwave sounders, atmospheric motion vectors, and scatterometers to provide wind radii and RMW estimates (Knaff et al., 2011). Additional details on these methods are listed in Table 4, including channels used, output resolution of the algorithms, mean errors of R34, caveats associated with each technique, suggested operational uses, and references.

Wind radii and possibly position and intensity (VMAX) derived from many of the methods discussed above are compiled into ATCF "fix deck" files (comma-delimited text data files) for use in U.S. operational TC forecast centers. ATCF system graphical user interfaces present fix deck file information to forecasters to aid real-time assessment, post-season analysis and other tasks. The fix deck file data are retained as a historical archive of the time, location, and surface wind structure elements extracted from satellite, aircraft, and algorithm/analysis. More information on the fix deck is available at (https://www.nrlmry.navy.mil/atcf_web/docs/database/new/newfdeck.txt). Other international forecast centers have developed similar databases, and users should check with those centers to determine availability and specifics on their individual records.

3.3. Emerging capabilities

Several other satellite algorithms for measuring TC surface winds have recently been introduced to operational

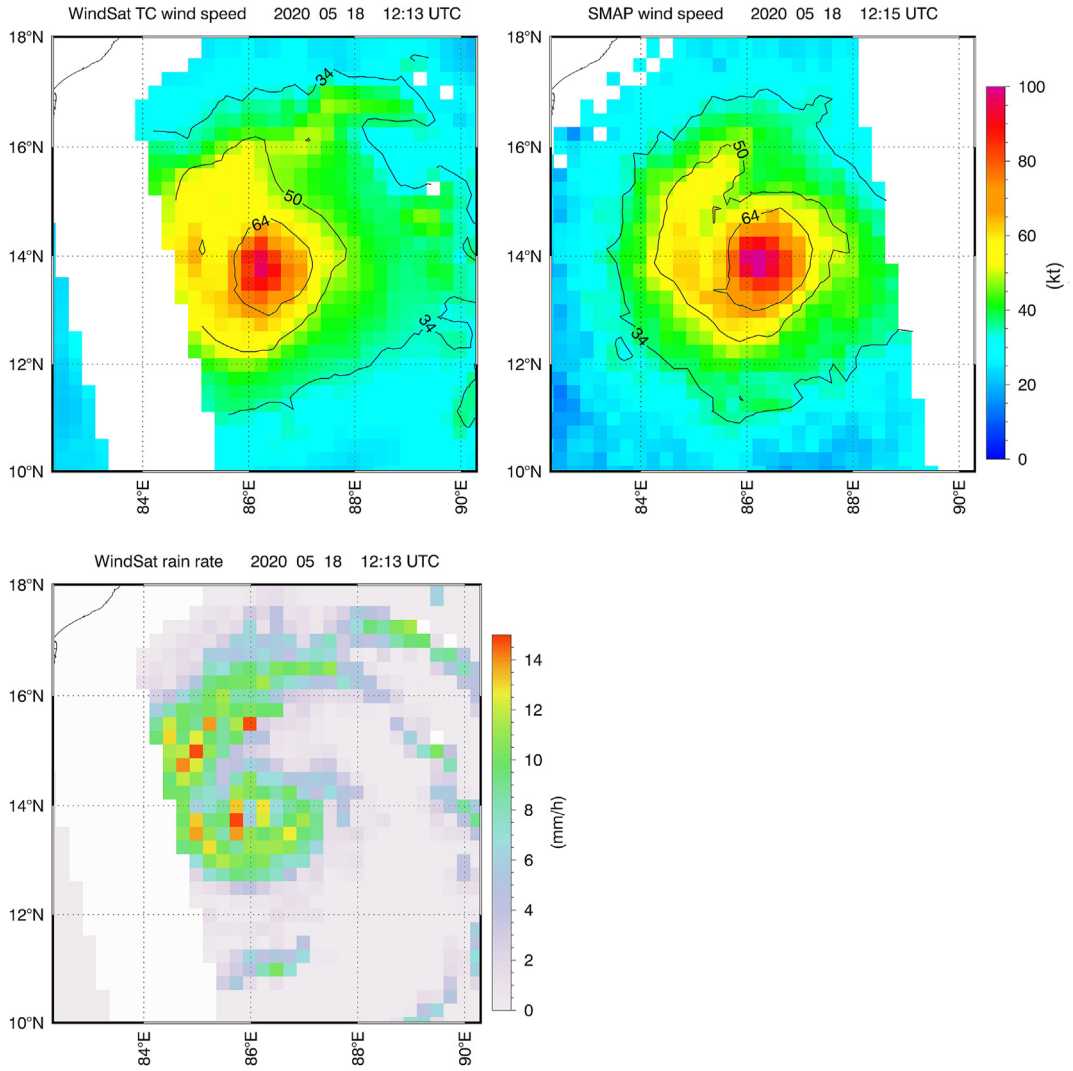

Fig. 5. (a) SMAP wind speeds (b) WindSat all-weather winds, and (c) WindSat rain rate for Tropical Cyclone Amphan in the Bay of Bengal at 12 UTC on May 18, 2020. Contours of 33, 25.7, and 17.5 $ms^{-1}$are shown in the top two panels for comparison.

forecasters. These include spaceborne synthetic aperture (active) radars (SARs), WindSat all-weather wind speeds, and Global Navigation Satellite System Reflectometry (GNSS-R).

3.3.1. SAR

Since the first SAR, SEASAT (NASA, 1978), ocean surface wind retrievals (Monaldo et al., 2003; Dagestad et al., 2012) have improved for speeds less than 70 kt (35 ms^{-1}) with development efforts applied specifically to TCs (Gonzalez et al., 1982; Katsaros et al., 2000). Most past SARs operate in co-polarization mode similar to ASCAT, which decreases sensitivity to wind speeds greater than 70 kt (35 m s^{-1}). Again, a co-polarized radar emits and receives in a single polarization. But starting with RadarSat-2 (CSA, 2007), SARs also have a cross-polarized mode that is more sensitive to extreme wind speeds found in TCs (Zhang et al., 2012; Horstmann et al., 2015; Hwang et al., 2015). A cross-polarized signal is collected when the SAR emits the signal in one polarization and receives in the other. The typical cross-polarized mode collects both co- and cross-polarized data in an alternating fashion. Three follow-on satellites, called the RadarSat Constellation Mission (RCM; Thompson, 2015) were launched in June of 2019 and declared operational on December 20, 2019. Copernicus—the European Union's Earth Observing Programme—also operates Sentinel 1A (2014) and 1B (2016), and provides acquisitions free of charge. Sentinel −1 A/B have co- and cross-polarization SAR capabilities that have been used to reconnoiter TC surface winds speeds, and combined co-polarized (lower wind speeds) and cross-polarized (higher wind speeds) SAR algorithms (Mouche et al., 2017). That SAR wind speed algorithm output is based on 3-km averages of SFMR wind speeds. Sentinel-1's, RadarSat-2 and RCM SARs are capable of measuring winds up to 150 kt (75 m s^{-1}) with errors comparable to those of SFMR data (Mouche ta al. 2019). There are signs of signal attenuation in the heaviest rain (>80 mm h^{-1}), but such attenuation can be filtered out via image processing methods described in Koch (2004), which are currently being

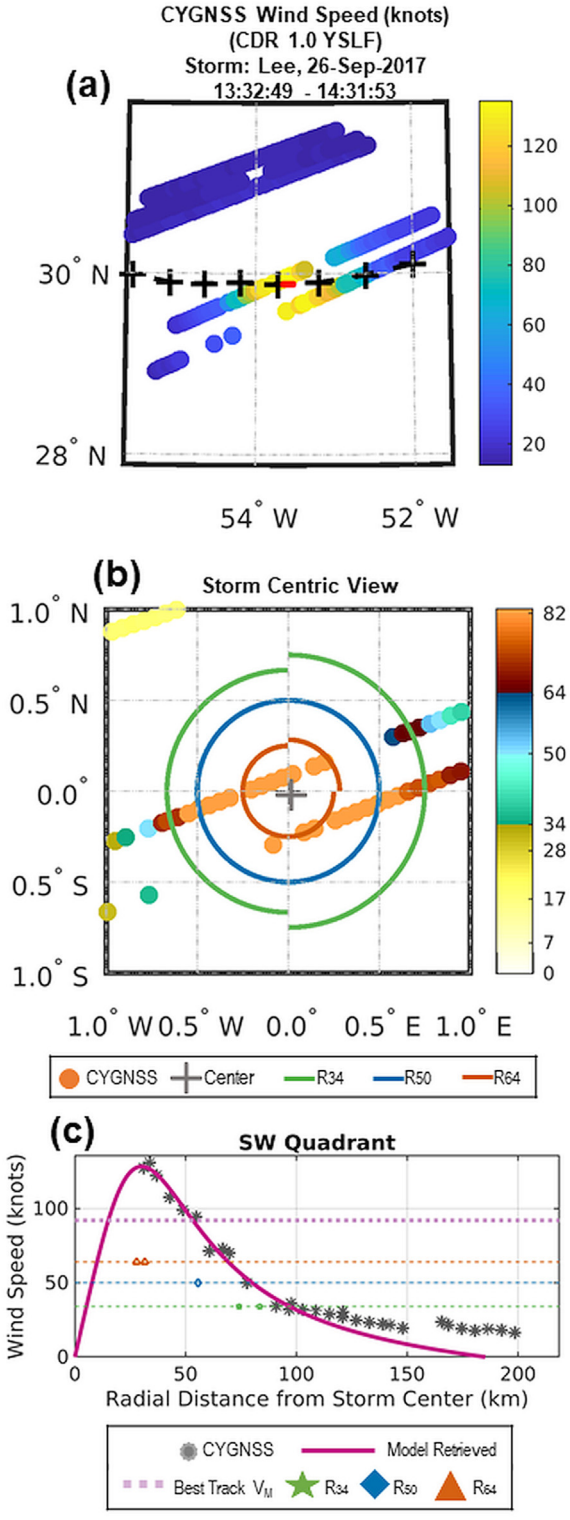

Fig. 6. A CYGNSS overpass of Hurricane Lee on September 26, 2017. (a) CYGNSS wind speed product (kt) where dashed-cross line denotes best track locations and red dots denote the interpolated center position during the CYGNSS pass. (b) CYGNSS wind speed (kt), but projected in storm centric coordinates, with the closest-in-time wind radii estimates visualized for comparison. (c) CYGNSS parametric model retrieval for all quadrants.

considered for operational application. Fig. 4a and b shows two SAR passes of Tropical Cyclone Veronica (2019) separated by 24 h. Fine details are evident in the imagery including polygonal eyewall features (Schubert et al., 1999) and the rotation of the maximum winds, marked by x's, from left of TC clockwise to the front and right as Veronica approached land. Fig. 4b also shows the effect of rain attenuation in the southeast quadrant, where winds drop from ~50 m s^{-1} (reds) to ~30 m s^{-1} (greens) over a span of about 20 km just outside the RMW. These images show that SAR's instantaneous wind field provides all of the information needed to estimate VMAX, RMAX, R34, R50, and R64.

The main limitation of SAR is its sporadic availability. Unlike most satellites in low Earth orbit that continuously collect and broadcast data, SARs are operated following predefined acquisition plans as these radars are operated in different exclusive modes. Any modifications of this plan requires specific request to change the mission, typically two to three days ahead of any acquisition. Data policy is different depending on agency. Radarsat-2 data is fee for service while Sentinel-1 data are free. To collect Sentinel-1 SAR passes over TCs, requests must be submitted through the Copernicus Emergency Management Service. Similarly, RadarSat-2 and RCM data have to be ordered through the Canadian Space Agency via MDA Ltd. Efforts within the WMO and Institut Français de Recherche pour l'Exploitation de la Mer (IFREMER) are underway to formalize SAR acquisitions over TCs as done for Mouche et al. (2017), where TC observations from the Satellite Hurricane Observations Campaign collected SAR data over TCs from 2016 to 2018. While SAR passes will become more common in the future, latency[3] and scheduling issues will continue to limit operational use. Archived RadarSat-2, RMC, and Sentinel-1 passes are available publicly for post-storm analysis and research from both NOAA and IFREMER, as described in the data availability statement.

3.3.2. All-weather wind speeds

WindSat employs the same channels as AMSR2, less the 89 GHz channel, so its wind speed algorithm also suffers from rain contamination (Meissner and Wentz, 2009). As with AMSR2, rain contamination can be mitigated by combining data from C-band and X-band channels that have both vertical and horizontal polarization (Meissner and Wentz, 2009; Zabolotskikh et al., 2015). These "all-weather wind speed" algorithms can be developed using SMAP wind speeds as ground truth because SMAP and WindSat have similar ascending times (approximately 18:00 Local) resulting in a large number of nearly-coincident WindSat and SMAP cases. Remote Sensing Systems (RSS) is currently training their WindSat algorithm to produce all-weather wind speed estimates with promising results (Meissner et al., 2021; Manaster et al., 2021). Fig. 5 shows a comparison between SMAP (Fig. 5a) and WindSat all-weather winds (Fig. 5b) in the case

[3] Within the last year, several RadarSat-2 TC wind speed estimates have been provided to JTWC within 2 h of acquisition.

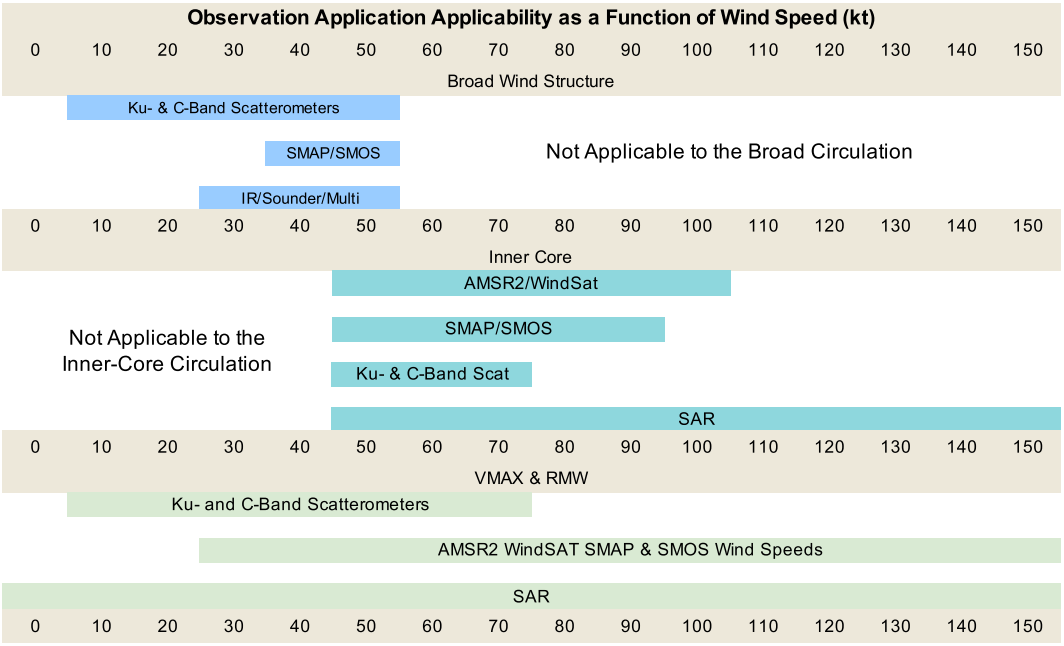

Fig. 7. Suggested uses for satellite-based sensors for determining operational estimates of TC structure, specifically the broad circulation, inner-core structural features, and those associated with the VMAX and RMW. Guidance is applicable for average size TCs.

of Tropical Cyclone Amphan in the Bay of Bengal at 12 UTC on May 18, 2020. Wind speeds are similar, even in the presence of extreme rainfall as indicated by the WindSat rain rate estimates (Fig. 5c). Such estimates complement other sensor data, providing additional temporal and spatial coverage. WindSat data unfortunately is no longer available, but an all-weather algorithm is a possibility for the U.S. Department of Defense's Weather Satellite Follow-on mission (WSF-M; Ball, 2019; OEPortal, 2020). Because SMAP wind speeds were used to train the algorithm, wind speed ranges and errors from the WindSat all-weather wind speed algorithm are expected to be similar to those of SMAP (Table 3).

3.3.3. GNSS-R techniques

GNSS-R is a remote sensing technique that uses L-band navigation satellite signals, specifically those that reflect from a surface. Reflection of the signal between the transmitting and receiving satellites provides a time delay and a frequency change—a Delay Doppler Map. The Delay Doppler Map's shape and power distribution over an ocean area is dictated by two reflecting surface conditions: the ocean's dielectric properties (known) and its roughness state, which is related to the wind speed (Zavorotny et al., 2014).

A current NASA mission, the Cyclone Global Navigation Satellite System (CYGNSS), is testing the GNSS-R technology. CYGNSS uses a constellation of eight microsatellites (SmallSats weighing 10–100 kg), each with a 4-channel GNSS-R radar receiver capable of measuring L-band (specifically L1 or 1.6 GHz) Global Positioning System (GPS) signals scattered from the surface (Ruf et al., 2016a, b; 2019; NASA 2020). CYGNSS retrievals are confined to very narrow swaths across the ocean surface (Ruf et al., 2019; Ruf and Balasubramaniam, 2018; CYGNSS, 2019). The demonstrated wind speed observation range for GNSS-R is 20–140 kt (10–70 m s^{-1}) with errors up to 12 kt (6 m s^{-1}). CYGNSS sampling depends on both CYGNSS and GPS satellite orbits, and is therefore a function of latitude, and time and space window choices (Bussy–Virat et al., 2018). The use of multiple microsatellites in a constellation increases both areal coverage and revisit times. Morris and Ruf (2017a, b) have developed objective methods to estimate TC intensity, wind radii, RMW, and integrated kinetic energy from CYGNSS wind speed estimates. The Morris and Ruf parametric model interpolates across tracks of CYGNSS observations through a storm, generating objective estimates of TC surface wind structure. Fig. 6a shows an example of CYGNSS coverage in Hurricane Lee (2017), a storm centric view (Fig. 6b) and outputs of the Morris and Ruf parametric model, Fig. 6c. CYGNSS provides fine resolution wind estimates only within the sensor's coverage areas (swaths), whereas the parametric model provides RMW, intensity, and wind radii. CYGNSS winds were initially adversely affected by variable signal strength from the GPS satellites that CubeSat design had not accounted for.

In addition to CYGNSS, the commercial spaceborne Earth observation sector has begun to launch low-cost SmallSats for a variety of applications. For example, Spire Global, Inc. launched and operated a constellation of 84 3U CubeSats with at least 30 focused on GNSS science and observations (Masters et al., 2019) as of December 2019. Effectively using data from all these relatively inexpensive SmallSats remains a challenge for developers and operators. If real-time capabilities are added, temporal and spatial coverage of oceanic winds would be enhanced beyond what is shown in Fig. 6a.

3.4. Archive data sets

Algorithm development, climatology studies, and other basic research all rely on archive data sets, and archive owners often seek partnerships with prospective users. Surface wind data archives are particularly useful given their operational relevance and the long history of surface wind measurements in both operations and experiments.

NOAA's Hurricane Research Division (HRD) maintains an archive of both NOAA research data and operationally-collected data from both NOAA and U.S. Air Force hurricane aircraft reconnaissance. Several reconnaissance datasets, including reprocessed SFMR, flight-level meteorological observations, dropwindsondes, and unmanned aerial vehicle observations, as well as derived products, are available from HRD's website. These datasets and products complement ATCF forecast, advisory, and satellite fix databases in tropical cyclone analysis and research applications. HRD also developed a surface wind analysis called H*Wind that synthesized ship, buoy, SFMR, and flight level wind observations (Powell et al., 1998). In 2014, H*Wind was transferred to Hwind Scientific, which is now part of Risk Management Systems. Analyses are available by request for scientific use (https://www.rms.com/event-response/hwind).

A number of remotely sensed datasets are available in addition to the previously cited SAR archives. NASA hosts a TC-focused archive for QuikScat data on the Jet Propulsion Laboratory's Tropical Cyclone Information System web site, which also includes experimental data from several other instruments (when available). Data in the QuikScat archive are reprocessed version 3 of the science quality data (SeaPAC, 2013; Fore et al., 2014), which have been further processed (Stiles et al., 2014) to capture higher TC winds and transform them into azimuthal averages (Chavas and Vigh, 2015). Other archived remotely sensed data sources include KNMI's scatterometer database and NOAA NESDIS's Ocean Surface Winds Team archive of scatterometer and radiometer surface wind display products. RSS maintains a reprocessed radiometer and scatterometer archive. The website URLs for accessing archived datasets are provided in data availability statements from each of the hosting organizations. We recognized there are many other Universities and organizations that provide similar datasets, but have limited this section to the most used of datasets.

3.5. Application to operations

Although it is advantageous to understand the nuances of individual observing systems and algorithms, forecasters require additional guidance regarding practical application of datasets to specific analysis requirements. Here we address considerations associated with applying the datasets to TC analysis following storm structure, starting from the outside and moving inward toward the TC core.

3.5.1. Broad TC wind structure

Ku- and C-band scatterometers are the primary source of observations for assessing 10–50 kt (5–25 m s^{-1}) surface winds over water, which are typically associated with the broader TC circulation. When available, these scatterometers provide estimates at 12.5–25 km grid points. The wind speed signal is most accurate below 50 kt (25 m s^{-1}) and in the absence of rain in the case of Ku-Band instruments (Donelan et al., 2004; Hwang et al., 2013; Hwang and Fois, 2015; Sapp et al., 2016). Multi-banded radiometers such as AMSR2 and WindSat can also be useful in these wind speed ranges (Alsweiss et al., 2018), and have the advantage of observing large coverage areas at adequate resolutions. Forecasters should avoid using data from L-band radiometers such as SMAP and SMOS for analyzing wind speeds less than 30 kt (15 m s^{-1}) as these sensors suffer from noise and low sensitivity at these low wind speeds. Using scatterometry augmented by radiometer-based (e.g., AMSR2) wind speed estimates to fill the spatial and temporal gaps is an optimal approach to wind analysis. If aircraft reconnaissance is available, SFMR can offer an independent data source. SFMR error standard deviations are 5–11 kt (2.4–5.6 m s^{-1}) at wind speeds below 50 kt (25 m s^{-1}) in light rain (Sapp et al., 2019). R34 and R50 estimates can be garnered from these data, either objectively or through visual inspection.

TC-specific algorithms based on microwave sounder, IR imagery, and multi-platform technique also provide R34 estimates. Beware that these algorithms prescribe structures to TCs and make assumptions about structure that are more applicable to TCs of higher intensity. These algorithms also provide estimates of R50 and R64, but such estimates still need validation, as errors are not well known. Fig. 7 provides current guidance on best practices to determine broad circulation (less than 50 kt or 25 m s^{-1}) from satellite-based methods.

When multiple objective wind radii estimates are available in a 6-h period, forecasters can use an equally weighted average of the estimates to reduce fluctuations in R34 through time (Sampson et al., 2017, 2018). Despite lower skill, the infrared, microwave sounder, and multi-platform technique wind radii estimates are sometimes included in these averages to improve temporal consistency in wind radii estimation. One can also attempt to apply weights based on errors associated with each method to provide higher quality average estimates.

3.5.2. Inner-core winds

As TCs intensify beyond 50 kt (25 m s^{-1}), eyewalls become evident (Vigh et al., 2012) and horizontal wind gradients steepen. Two factors complicate satellite wind observation in the areas where steep wind speed gradients are present: sensor resolution and sensitivity. Aircraft reconnaissance with both flight level and SFMR winds is the primary choice for measuring high wind speed gradients, but such measurements are rarely available outside the North Atlantic. The signal of higher frequency radiometers (e.g., AMSR2 and WindSat) remains sensitivity to winds exceeding 50 kt

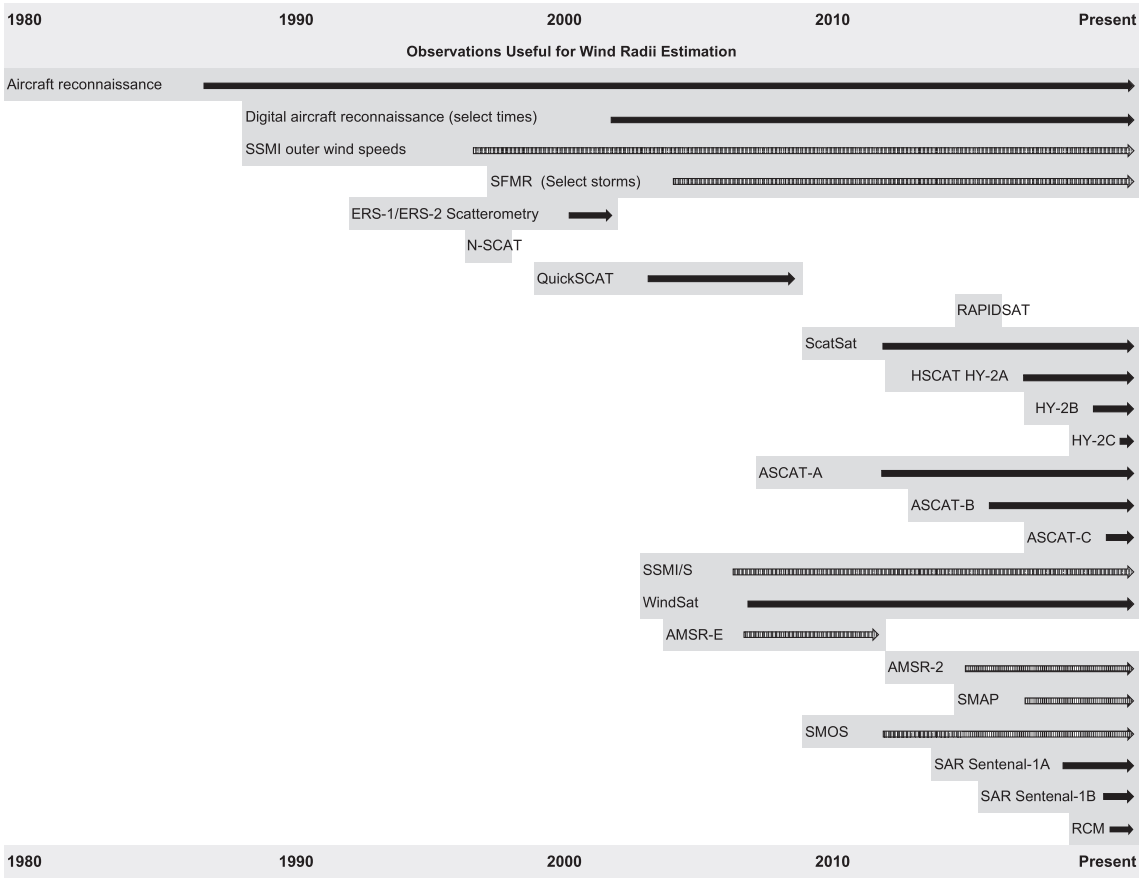

Fig. 8. Observations available in near real-time on operational workstation, data repositories, or web sites for estimating tropical cyclone surface wind structure. Noting that availability on operational workstations, which varies among agencies, likely ensure they could have been used for post-storm analysis. Thus, this timeline represents the best scenario. Gray areas provide the starting/ending time, solid (hatched) arrows indicate wind vector (wind speed) estimates. Gray horizontal areas (including text and arrows) indicate the time periods during which annotated information was available.

(25 m s^{-1}) without attenuation and can provide valuable information about the areal coverage of winds exceeding 50 kt (25 m s^{-1}). AMSR2 provides more useful information than WindSat at higher wind speeds because AMSR2 has an 89 GHz channel that better mitigates the effects of heavy rain. The use case for these sensors are limited mostly by resolution, and in most cases, except small[4] TCs, can provide 2-D surface wind information to speeds up to 100 kt (50 m s^{-1}). C- and Ku-band scatterometers provide wind vectors that are most useful for estimating R50 since they are co-polarized and lose sensitivity at wind speeds higher than 50 kt (25 m s^{-1}). The two L-band sensors SMAP and SMOS, while unaffected by rainfall or saturation issues, are limited by coarser resolution, and subjectively provide structure guidance up to about 90 kt (46 m s^{-1}), conservatively, in average-sized storms. Nonetheless, these L-band sensors dramatically improve temporal detection of these higher wind speeds despite resolution issues and increased error in areas where fresh water flows into the ocean (Reul et al., 2016, 2017; Yueh et al., 2016, Meissner et al., 2017).

Finally, SAR wind speeds are invaluable, as instantaneous winds can be measured up to 150 kt (70 m s^{-1}) at 3 km or higher resolution (Mouche et al., 2019). Determining time-averaged winds from instantaneous SAR wind data is challenging. Recent study has shown that a 3-km wind average is well correlated (R = 0.92) with small biases (−0.4 kt; −0.2 m s^{-1}) to 1-min sustained winds estimated from SFMR (Combot et al., 2020). Fig. 7 provides suggested uses of the satellite-based methods for average-sized[5] TCs in the inner core where winds are typically near or slightly below 50 kt (25 m s^{-1}). Users should be cognizant that wind speeds estimates at coarse resolutions essentially represent a weighted area average of the wind field, and in the steep horizontal wind gradients, like in small TCs, cannot be resolved resulting in both lower maxima and higher minima than could be captured at finer resolutions.

3.5.3. VMAX and RMW

Estimating TC intensity, or VMAX, is also an important part of the TC advisory process since it is often used to

[4] ROCI <165 n mi (Knaff et al., 2016).

[5] 165 n mi ≤ ROCI <270 n mi (Knaff et al., 2016).

classify the TC and to initialize various prediction models. In situ observations are difficult to obtain due to both the severity and small size of the extreme winds. Aircraft-based observations are critical to the NHC forecast process, but these observations are generally limited to the North Atlantic near land. Fortunately, there are effective and reliable methods to estimate VMAX in most situations when aircraft data are not available. The subjective (Dvorak, 1984; Velden et al., 2006) and automated (Olander and Velden, 2019) Dvorak techniques have provided estimates of VMAX for decades. Intensity estimates from microwave imagers and sounders complement the Dvorak-based information (Brueske and Velden, 2003; Demuth et al., 2004; Herndon and Velden, 2014). Routine Dvorak and Satellite Consensus estimates (SATCON; Velden and Herndon, 2020) typically provide reasonable first guesses at TC intensity, with root mean square errors (RMSEs) of 4–12 kt/2–6 m s^{-1} (Knaff et al., 2010). NHC forecasters generally favor aircraft reconnaissance data from flight-level and SFMR, if available, over satellite estimates for determining VMAX. If the initial VMAX estimate is below 70 kt (35 ms^{-1}), co-polarized, both Ku- and C-Band scatterometry may be considered, with more scrutiny being applied to Ku-Band instruments in heavy rain. Above 30 kt (15 ms^{-1}), surface winds from multi-band and L-band radiometers are applicable. The L-band wind algorithms produce data with resolution similar to the size of a RMW, and provide a lower limit (floor) to VMAX when the RMW is less than 25 n mi (47 km), the 25th percentile (Kimball and Mulekar, 2004). Additionally, 3-km averaged co- and cross-polarized SAR winds provide a reasonable basis for estimating VMAX, with high correlations (>0.90), small biases (<3%) and RMSEs less than 10 kt (5 m s^{-1}) when compared to SFMR observations (Combot et al., 2020). In basins where SFMR observations are unavailable, correlations between SAR winds and quality-controlled final best track analysis data are still large (≥0.85) with biases of −1.3–3% and RMSEs of 12–16 kt (6–8 m s^{-1}).

RMW estimates are often required at TC forecasting centers, and they are challenging to construct due to limited high quality observations in the inner core. SFMR-based and flight-level estimates of RMW can be quite different between the inbound and outbound radial legs, and subjective analysis is often still necessary. The best data source for RMW, when available, is the co- and cross-polarized SAR. The SAR sensor provides an instantaneous fine-scale snapshot of the entire inner-core wind field. When available, SAR images depict accurate estimates of RMW, VMAX, VMAX location and operationally important wind asymmetries as shown in Combot et al. (2020), with good correlation (>0.70) and small root mean square errors (<12 km) relative to SFMR. These relationships improve significantly if heavy rainfall near the eyewall can be removed from the data retrieval (Combot et al., 2020). High-frequency radiometers can provide additional RMW information, especially for large [> 40 n mi (75 km)] TC RMWs. In TCs with winds below ~50 kt (25 m s^{-1}), forecasters can use wind data from scatterometers and high frequency radiometers to estimate RMW. Scatterometer data are exceptionally useful for analyzing the wind field in TCs undergoing formation, although TCs with very small [< 15 n mi (28 km), the 10th percentile (Kimball and Mulekar, 2004)] RMWs early in development (Mallen et al., 2005, their Fig. 5) present an additional challenge. Routine accurate estimates of RMW from remotely sensed data will likely remain a challenge for operational forecasters.

4. Historical perspective, needs, and recommendations

4.1. Historical perspective

To understand the quality of best track wind radii information, we need to examine observation availability through time (Fig. 8). Prior to 1988, only wind speed observations of opportunity were available to operational TC forecasting centers. The Special Sensor Microwave Imager (SSM/I), which provided passive microwave data applicable for estimating wind speeds in rain free regions, began retrievals in 1987. The following year, aircraft data transmission latency decreased as satellite-based transmission of aircraft reconnaissance information such as center fixes, which provided central pressure estimates. Flight-level wind measurements remained unreliable in this period.

By the 1990s, scatterometer winds became available to operational forecasters. The European Space agency launched the first C-band scatterometers on ERS-1 and -2, each with narrow swaths of approximately 500 km and 25 km grid spacing. Unfortunately, operational application of these early scatterometer data is not well-documented, but was available at JTWC around 1996 (e.g., Sampson and Schrader, 2000). The NASA scatterometer (NSCAT), with two 600-km swaths separated by a 330-km data gap, became the first Ku-band scatterometer that was clearly referenced by TC forecasters. NSCAT was launched on the Advanced Earth Observing Satellite (ADEOS) on August 16, 1996 (Graf et al., 1998). Although NSCAT failed on June 30, 1997, operational forecasters accepted and used NSCAT data until its demise. QuikScat, the NSCAT "quick recovery" replacement, launched on June 19, 1999. QuikScat was a Ku-band scatterometer with an 1800 km data swath (see Table 3 for more details). QuikScat data was available real-time by 2000, and provided reliable surface winds for approximately 10 years (Brennan, 2009).

Several advancements in satellite-based surface wind observation occurred in the 2000s, including the launch of WindSat and AMSR-E radiometers. Although WindSat wind vectors were of limited use in high winds, and AMSR-E was not used for wind speed estimation, reliable data availability for both sensors eventually led to development of all-weather AMSR2 and WindSat wind speed algorithms. In 2006, the European Organisation for the Exploitation of Meteorological Satellites (EUMETSAT) launched its first operational ASCAT on the Metop-A satellite. ASCAT missions continue to this day, with sensors onboard three satellites routinely providing reliable data within 550 km wide swaths along their orbital paths. ASCAT remains critical to operational forecasters,

providing R34 and R50 estimates and VMAX for weaker systems. OceanSat-2 carried a Ku-band scatterometer with its launch in 2009, boosting temporal and spatial coverage over global oceans just as QuikSCAT reached its end of service.

Developments in scatterometry, wind retrieval algorithms and synthetic aperture radar continued throughout the 2010s and into the early 2020s. China launched the Haiyang-2 satellite series (HY-2A, -B and −C), beginning with HY-2A in 2011. HY-2C, launched in 2020, is in an inclined non-sun-synchronous orbit, which should help with its temporal coverage. Information on HY-2 Ku-band scatterometers' TC-monitoring capabilities is somewhat limited (Zhao et al., 2016; Zhao and Zhao, 2019), but cursory viewing suggests that the Haiyang-2 series has performance similar to that of other Ku-band scatterometers. The RapidScat Ku-band scatterometer had a limited lifespan (2014–2016) and provided observations from the International Space Station (NASA, 2021). SCATSAT launched in 2016, and employs the same type of Ku-band scatterometer as its OceanSat predecessor. OceanScat-2 scatterometer data were recently calibrated for TCs, but still present interpretation challenges. In 2019 and 2020, wind speed algorithms for L-band radiometers such as SMOS and SMAP gained acceptance at JTWC and other operational centers. Starting in 2019, RadarSat-2, Sentinel-1, and the RCM SARs all now provide high-resolution surface winds for operational centers. While many operational centers are evaluating the plethora of recently available satellite capabilities, they all still rely heavily or entirely (NHC) on ASCAT.

4.2. Emerging capabilities

The future of TC surface wind field observations is bright. Scatterometers from China, India, and the European Union are scheduled for launch, likely extending scatterometer wind data availability for the foreseeable future. The EUMETSAT Polar System Second Generation Scatterometer will include both co- and cross-polarization and, similar to SAR, will be sensitive to high wind speeds (Rostan et al., 2019; Stoffelen et al., 2017b). Several radiometers designed to observe over-ocean winds are planned for launch, including the Copernicus Imaging Microwave Radiometer (Kilic et al., 2018), the Compact Ocean Wind Vector Radiometer (Brown et al., 2017) and the US Air Force's WSF-M (Ball, 2019; OEPortal, 2020), which also includes non-microwave weather sensing options. The future of SAR is probably the most promising, with the recently launched RCM, two planned Sentinel missions (Sentinel 1C and 1D), and one planned NASA L-band/S-band SAR (NISAR; Rosen et al., 2017) mission. NISAR's L-band SAR is similar to the active sensor on SMAP (Fore et al., 2019), although routine acquisition for TCs is still being formalized. GNSS-R technology (e.g., CYGNSS) is also promising, especially since the sensors can reside on inexpensive spacecraft constellations instead of the more expensive spacecraft that are required to carry active radars or large passive L-band radiometers. SmallSat constellations that sense the 118-GHz oxygen window, such as the sensor flown on the Chinese Feng Yun-3C satellite, may also provide information that can be used to estimate intensity and wind radii. The latter will be tested in the Time-Resolved Observations of Precipitation structure and storm Intensity with a Constellation of SmallSats (TROPICS, 2019) and the Global Environmental Monitoring System (GEMS, 2020). The TROPICS mission is targeted for launch between January 8 and July 31, 2022, but a pathfinder mission was launched June 30, 2021, and GEMS is scheduled to follow up on an earlier prototype with a launch in the December 2021. GEMS will provide real-time data, but unfortunately, TROPICS and many other SmallSat missions will likely provide data with lengthier time delays.

4.3. Recommendations

Current capabilities are insufficient to support specification of the entire TC surface wind field every 6 h, as TC forecasting centers require. And, forecasters need more timely data with higher temporal and spatial resolution (on the order of 2–4 km) to identify features such as secondary wind maxima and eyewall replacement cycles. Researchers and product developers also need accurate records of all relevant TC surface wind parameters in best track and other operationally-generated datasets in order to develop high-quality analysis guidance and conduct climatological studies. These requirements lead us to provide four recommendations, indented and italicized in boldface below.

Current TC wind field estimates, while improved, are insufficient to address the requirements described above. To determine specific observational requirements, we start with the parameters and frequency of reporting that are required in operations. Vigh et al. (2012) reported that RMWs can be as small as 2 n mi (4 km) while Weatherford and Gray (1988) reported that R34s can be as large as 600 n mi (1100 km). Most advisories and forecasts are issued at 6-h intervals. Based on these considerations,

> *surface wind data coverage from a combination of sources should cover an area extending at least 600 n mi (1100 km) from TC centers with a horizontal resolution on the order of 2 km in the inner-core region, and be available at least every six hours.*

This ambitious frequency and horizontal resolution would satisfy current operational needs and could be used as a guide for future observation system design requirements. And, as we have witnessed with the lack of real-time capabilities of CYGNSS and TROPICS mission, it is difficult to get operational forecasters engaged in the evaluation process. Thus, we recommend that

> *planning for research and experimental observational capabilities (*e.g.*, for surface wind estimation) should incorporate adequate funding for instrument design and ground station capabilities so that near real-time digital data are provided for forecasting applications and critical evaluation during real-time weather events.*

Operational users and researchers can and will provide feedback on new capabilities, especially capabilities that address operational needs and missions.

Fig. 8 shows a history of availability for the remotely sensed data used for TC surface wind estimation. The historical record raises concern about the quality of wind structure estimates in the best tracks before 2000, as the data available to inform such estimates are sparse or non-existent. Post-season reanalysis (of best track datasets) is inherently subjective, and the type and quality of historical data available to inform surface wind field estimates, even since 2000, are highly variable. On the bright side, observation availability and operational capabilities have improved in the last 15–20 years, so the more recent estimates in the best tracks are more likely to be based on observations. In fact, many TC centers are just beginning to conduct rigorous post-season analysis of their best track wind radii. Documentation on post-season analyses of wind radii has been provided for North Atlantic and eastern North Pacific (Landsea and Franklin, 2013), the Australian Region (Bureau of Meteorology, 2020; Courtney et al., 2020), and western North Pacific TCs (Sampson et al., 2017; JMA, 2020). Still, there are homogeneity issues in the analyses and users need to understand the quality and background of these best track analyses before using them for research and development. Uncertainties in wind radii estimates have been discussed in Sampson et al. (2017, 2018) and Combot et al. (2020). It is also important that while these data were available for post-storm analyses (Fig. 8), the availability of data on operational workstations, which implies it could have been used for such analyses, varies greatly from agency to agency. Organizational staffing and priorities also may impact the quality of such analyses. Thus, Fig. 8 presents a record of what could be used in a thorough reanalysis from all the past data. Because of these many issues,

Best track users should contact organizations that created the records in order to properly assess whether datasets are appropriate for their use.

Despite recent and ongoing efforts to quality control surface wind best track records, there is a pressing need to acquire quality databases of wind speed estimates (section 3e) for use in research and development. However, the dearth of oceanic wind data prior to the early 2000s (Fig. 8) suggests that, with the data currently available that

Wind radii reanalysis efforts should begin no earlier than the early 2000s.

This statement finds further support in recent efforts to reanalyze wind radii at the Bureau of Meteorology, which concluded that their highest quality best tracks exist for periods following the 2003–2004 season (Bureau of Meteorology, 2020; Courtney et al., 2020).

5. Summary and concluding remarks

In this review, we have described operationally-relevant TC wind structures, presented a brief history of operational practices and the associated climatological datasets, discussed tools available for estimating TC surface winds, and documented records available for studies. Optimal surface wind estimation techniques would estimate VMAX within the 10 kt (5 m s^{-1}) uncertainty observed in the best track (Landsea and Franklin, 2013; Torn and Snyder, 2012; Combot et al., 2020) and wind radii to within an 20% mean error (Sampson et al., 2017; Combot et al., 2020). Many of the remote sensing sensors cited in this review provide data useful to achieving these goals, but human intervention is typically required to discern the quality and capabilities of each.

Table 3 summarizes aircraft and satellite-based surface wind speed estimates that are currently available to operators for subjective analysis, many within 4 h of analysis time. Most are useful for assessing winds up to 50 kt (25 ms^{-1}), particularly ASCAT, HY-2, SMAP and SMOS. When the TC is large, SMAP and SMOS can provide valuable information about the extent of the 64-knot winds. Because of its higher resolution, AMSR2 provides valuable information about wind speeds near the core of TCs. These new sensors and algorithms dramatically increase the wind speed temporal and spatial coverage in TCs, and complement TC-specific algorithms designed to estimate wind radii (Table 4). While not the primary focus of this review, each of these data sources can also be used to analyze maximum intensity in operations, especially in cases when traditional methods (e.g., the Dvorak methods) are uncertain.

We have also discussed emerging data sources that augment spatial and temporal coverage of the wind fields. These include SAR, WindSat all-weather winds, and GNSS-R. SAR provides a nearly instantaneous snapshot of the surface wind speeds at up to 50 m resolution, along with a high-resolution snapshot of storm structure, including the RMW. More SAR data are becoming available to operations with the recent launch of the RCM, RadarSat-2, and ESA's Sentinel 1 A and B satellites, a current total six SAR platforms. And, Sentinel 1 C/D, and NISAR will provide two more in the near future. IFREMER and NOAA are acting to formalize agreements to collect and process SAR data over TCs on a routine basis. Thanks to ongoing efforts by those organizations, SAR data latency has dropped to as little as 2 h. However, SAR data acquisition reservations must be placed at least 48 h in advance, and are thus depend on forecast track accuracy to target the correct locations. RSS has demonstrated the capability to produce all-weather wind speed estimates from WindSat, which bodes well for future efforts with similar sensors. Though at present, the still-functioning WindSat's future is uncertain as the data is no longer available. NASA's GNSS-R demonstration has demonstrated that GNSS satellite constellations can be used to provide wind speed estimates over large areas on a small budget. Variability in GPS signals has challenged NASA's GNSS-R demonstration, and future efforts would need to mitigate this issue for all GNSS satellite constellations, but the outlook is promising. It is quite possible that GNSS-R winds will soon be available in operations from commercial sources.

In reviewing historical archives available to assess surface winds in TCs (Fig. 8) and the best track archives (Fig. 1), we made two specific recommendations that are highlighted in section 4.3. We concluded that the current state of TC surface wind analysis is improving, but still insufficient to meet operational needs. Even with planned launches, coverage will likely fall short of the operational requirement—specification of TC wind field from the outer 34-kt radii to the inner RMW at least every 6 h. However, the satellite hardware field is evolving at a rapid pace. The proliferation of SmallSats should continue to improve coverage and reduce latency. Ensuring usefulness of the data for the TC forecasting and research community must be a priority including real-time availability of experimental and research observing capabilities. SmallSat-based capabilities and continual improvements in algorithms with continuing aircraft reconnaissance providing critical, ground truth data sets for verification should move us closer to satisfying operational needs. For future observational network design, we have recommended an ambitious and likely expensive goal for future observations systems to meet the needs of TC operations. We hope that our community can and will learn to use the data from emerging sensors and platforms, including the inexpensive and ever-expanding population of SmallSats and newly-developed TC observation capabilities and algorithms.

Data availability statement

This publication is supported by multiple datasets, which are openly available, though for cyber security registration is often required. The following are data types followed by locations where data availability can either be directly accessed or registration for access can be initiated: AMSR2 wind speeds from JAXA at https://suzaku.eorc.jaxa.jp/GCOM_W/data/data_w_dpss.html, AMSR2 wind speed data from NOAA https://satepsanone.nesdis.noaa.gov/pub/product/nde/amsr2/L2/(contact Paul Chang, paul.s.chang@noaa.gov), AMSR2 wind speeds from Remote Sensing Systems at http://www.remss.com/missions/amsr, SMAP wind speeds from NASA at https://podaac.jpl.nasa.gov/dataset/SMAP_JPL_L2B_NRT_SSS_CAP_V42, SMAP wind speed from Remote Sensing Systems at http://www.remss.com/missions/smap/, SMOS wind speeds at https://www.smosstorm.org/Data2/SMOS-NRT-wind-Products-access, ASCAT, QuikScat, SCATSAT, HSCAT and other scatterometer data from http://projects.knmi.nl/scatterometer/home/, CYGNSS wind speed data at https://podaac.jpl.nasa.gov/CYGNSS?sections=data, SAR data from NOAA at https://www.star.nesdis.noaa.gov/socd/mecb/sar/AKDEMO_products/APL_winds/tropical/, SAR data from IFERMER at https://cyclobs.ifremer.fr/app/, Aircraft data including SFMR at https://www.aoml.noaa.gov/hrd/data_sub/hurr.html, and climate quality QuikScat data from NASA at https://tropicalcyclone.jpl.nasa.gov/.

Acknowledgments

J. Knaff thanks NOAA/Center for Satellite Applications and Research for providing the time to compile this review, and to attend the 9th International Workshop on Tropical Cyclones, where this idea has its origins. ONR has provided funding C. Sampson through Program Element 0603207N. M. Morris gratefully acknowledges support from the CYGNSS Science Team. Her work was supported as part of the CYGNSS Competed Science and a part of the work described in this paper was carried out by the Jet Propulsion Laboratory, California Institute of Technology under a contract with the NASA, Government sponsorship acknowledged. L. Ricciardulli and T. Meissner acknowledge funding by the NASA Team Science Utilization of the Soil Moisture Active-Passive Mission (SUSMAP, contract NNH17CA04C) and the NASA Ocean Vector Wind Science Team (OVWST, contract 80HQTR19C0003). Alexis Mouche's work was supported ESA through S1−4SCI Ocean Study project (Contract No. 4000115170/15/I-SBo), Sentinel-1 A Mission Performance Center (Contract No. 4000107360/12/I-LG), CHEFS EUMETSAT project and by public funds (Ministère de l'Education Nationale, de l'Enseignement Supérieur et de la Recherche, FEDER, Région Bretagne, Conseil Général du Finistère, Brest Métropole) and by Institut Mines Télécom, received in the framework of the VIGISAT project managed by "Groupement Bretagne Télédétection" (BreTel). Finally, N. Reul acknowledges the support of ESA in the frame of the SMOS Wind Data Service contract (http://www.smosstorm.org/). We would also like to thank Megan Fritz for assistance with references, Ed Rappaport, and Brian Zachary of the National Hurricane Center, David Schultz and the other five anonymous reviewers for their constructive comments on earlier versions of this manuscript. Finally we offer a special thanks to Chris Landsea and the anonymous reviewer for constructive comments on this manuscript. The views, opinions, and findings contained in this report are those of the authors and should not be construed as an official National Oceanic and Atmospheric Administration or U.S. Government position, policy, or decision.

References

Alpers, W., Zhang, B., Mouche, A., Zeng, K., Chan, P.W., 2016. Rain footprints on C-band synthetic aperture radar images of the ocean−revisited. Remote Sens. Environ. 187, 169−185. https://doi.org/10.1016/j.rse.2016.10.015.

Alsweiss, S., Sapp, J., Jelenak, Z., Chang, P., 2018. Validation of AMSR2 oceanic environmental data records using tropical cyclone composite fields. In: IGARSS 2018 - 2018 IEEE International Geoscience and Remote Sensing Symposium, pp. 3078−3081. https://doi.org/10.1109/IGARSS.2018.8517426. Valencia, Spain.

AMS Glossary of Meteorology, 2020. Bogus Vortex. http://glossary.ametsoc.org/wiki/Bogus_vortex. (Accessed 1 July 2020).

Anguelova, M.D., Webster, F., 2006. Whitecap coverage from satellite measurements: a first step toward modeling the variability of oceanic whitecaps. J. Geophys. Res. 111, C03017. https://doi.org/10.1029/2005JC003158.

Attema, E.W.P., 1991. The active microwave instrument on board the ERS-1 satellite. Proc. IEEE 79, 791−799.

Ball, 2019. Weather system follow-on microwave. https://www.ball.com/aerospace/Aerospace/media/Aerospace/Downloads/D3395_WSF-M_1217.pdf?ext=.pdf. (Accessed 27 May 2020).

Bettenhausen, M.H., Smith, C.K., Bevilacqua, R.M., Wang, Nai-Yu, Gaiser, P.W., Cox, S., 2006. A nonlinear optimization algorithm for WindSat wind vector retrievals. IEEE Trans. Geosci. Remote Sens. 44, 597−610. https://doi.org/10.1109/TGRS.2005.862504.

Black, P., McIntosh, R., Swift, C., Carswell, J., Germain, K. St, Popstefanija, I., Goodberlet, M., 1995. Ocean surface wind, stress, and rain rate measurements in tropical cyclones from concurrent airborne microwave scatterometer and radiometer measurements. In: Reprints of the 27th Conference on Radar Meteorology. AMS, Vail, CO, USA, pp. 623−625.

Bourassa, M.A., Meissner, T., Cerovecki, I., Chang, P.S., Dong, X., DeChiara, G., Donlon, C., Dukhovskoy, D.S., Elya, J., Fore, A., Fewings, M.R., Foster, R.C., Gille, S.T., Haus, B.K., Hristova-Veleva, S., Holbach, H.M., Jelenak, Z., Knaff, J.A., Kranz, S.A., Manaster, A., Mazloff, M., Mears, C., Mouche, A., Portabella, M., Reul, N., Ricciardulli, L., Rodriguez, E., Sampson, C., Solis, D., Stoffelen, A., Stukel, M.R., Stiles, B., Weissman, D., Wentz, F., 2019. Remotely sensed winds and wind stresses for marine forecasting and ocean modeling. Front. Mar. Sci. 6, 443−475. https://doi.org/10.3389/fmars.2019.00443.

Brennan, M.J., Hennon, C.C., Knabb, R.D., 2009. The operational use of QuikSCAT ocean surface vector winds at the National Hurricane Center. Weather Forecast. 24, 621−645. https://doi.org/10.1175/2008WAF2222188.1.

Brown, S., et al., 2017. The COWVR Mission: demonstrating the capability of a new generation of small satellite weather sensors. In: 2017 IEEE Aerospace Conference. IEEE, Big Sky, MT, USA, pp. 1−7. https://doi.org/10.1109/AERO.2017.7943884.

Brueske, K., Velden, C., 2003. Satellite-based tropical cyclone intensity estimation using the NOAA-KLM series Advanced Microwave Sounding Unit (AMSU). Mon. Weather Rev. 131, 687−697. https://doi.org/10.1175/1520-0493(2003)131%3C0687:SBTCIE%3E2.0.CO;2.

Bureau of Meteorology, 2020. Previous Tropical Cyclones. http://www.bom.gov.au/cyclone/history/index.shtml. (Accessed 20 April 2020).

Bussy-Virat, C.D., Ruf, C.S., Ridley, A.J., 2018. Relationship between temporal and spatial resolution for a constellation of GNSS-R satellites. IEEE J. Sel. Topics Appl. Earth Obs. Remote Sens. 12, 16−25. https://doi.org/10.1109/JSTARS.2018.2833426.

Chan, P.W., Hon, K.K., Foster, S., 2011. Wind data collected by a fixed-wing aircraft in the vicinity of a tropical cyclone over the south China coastal waters. Meteor. Z. 20, 313−321. https://doi.org/10.1127/0941-2948/2011/0505.

Chang, P., Jelenak, Z., Alsweiss, S., Sapp, J., 2015. Algorithm Theoretical Basis Document: GCOM-W1/AMSR2 Day-1 EDR, vol. 2, p. 22. https://www.star.nesdis.noaa.gov/jpss/documents/ATBD/ATBD_AMSR2_Ocean_EDR_v2.0.pdf. (Accessed 23 April 2020).

Chavas, D.R., Emanuel, K.A., 2010. A QuikSCAT climatology of tropical cyclone size. Geophys. Res. Lett. 37, L18816. https://doi.org/10.1029/2010GL044558.

Chavas, D.R., Vigh, J.L., 2015. QSCAT-R: the QuikSCAT tropical cyclone radial structure dataset. Tropical Cyclone Data Project, National Center for Atmospheric Research. https://doi.org/10.5065/D65B00J3.

Combot, C., Mouche, A., Knaff, J., Zhao, Y., Zhao, Y., Vinour, L., Quilfen, Y., Chapron, B., 2020. Extensive high-resolution Synthetic Aperture Radar (SAR) data analysis of tropical cyclones: comparisons with SFMR flights and best track. Mon. Weather Rev. 148, 4545−4563. https://doi.org/10.1175/MWR-D-20-0005.1.

Courtney, J.B., Burton, A., Velden, C.S., Olander, T.L., Ritchie, E.A., Stark, C., Majewski, L., 2020. Towards an objective historical tropical cyclone dataset for the Australian region. Tropical Cyclone Res. Rev. 9, 23−36. https://doi.org/10.1016/j.tcrr.2020.03.003.

CSA, 2007. RADARSAT−2. https://www.asc-csa.gc.ca/eng/satellites/radarsat2/Default.asp. (Accessed 1 May 2020).

CYGNSS, 2019. CYGNSS. https://www.nasa.gov/cygnss. (Accessed 17 September 2021).

Dagestad, K.-F., Horstmann, J., Mouche, A., Perrie, W., Shen, H., Zhang, B., Li, X., Monaldo, F., Pichel, W., Lehner, S., Badger, M., Bay Hasager, C., Furevik, B., Foster, R.C., Falchetti, S., Caruso, M.J., Vachon, P., 2012. Wind retrieval from synthetic aperture radar − an overview. In: Proceedings of SEASAR 2012. European Space Agency, Tromso, Norway, p. 22.

Demuth, J.L., DeMaria, M., Knaff, J.A., 2006. Improvement of Advanced Microwave Sounding Unit tropical cyclone intensity and size estimation algorithms. J. Appl. Meteorol. 45, 1573−1581. https://doi.org/10.1175/JAM2429.1.

Demuth, J.L., DeMaria, M., Knaff, J.A., Vonder Haar, T.H., 2004. Evaluation of advanced microwave sounding unit (AMSU) tropical cyclone intensity and size estimation algorithm. J. Appl. Meteorol. 43, 282−296. https://doi.org/10.1175/1520-0450(2004)043%3C0282:EOAMSU%3E2.0.CO;2.

Depperman, C.E., 1947. Notes on the origin and structure of Philippine typhoons. Bull. Amer. Meteorol. Soc. 28, 399−404.

Dolling, K., Ritchie, E.A., Tyo, J.S., 2016. The use of the Deviation Angle Variance Technique on geostationary satellite imagery to estimate tropical cyclone size parameters. Weather Forecast. 31, 1625−1642. https://doi.org/10.1175/WAF-D-16-0056.1.

Domingues, R., Kuwano-Yoshida, A., Chardon-Maldonado, P., Todd, R.E., Halliwell, G., Kim, H.-S., Lin, I.-I., Sato, K., Narazaki, T., Shay, L.K., Miles, T., Glenn, S., Zhang, J.A., Jayne, S.R., Centurioni, L., Le Hénaff, M., Foltz, G.R., Bringas, F., Ali, M.M., DiMarco, S.F., Hosoda, S., Fukuoka, T., LaCour, B., Mehra, A., Sanabia, E.R., Gyakum, J.R., Dong, J., Knaff, J.A., Goni, G., 2019. Ocean observations in support of studies and forecasts of tropical and extratropical cyclones. Front. Mar. Sci. 6, 446. https://doi.org/10.3389/fmars.2019.00446.

Donelan, M., Haus, B., Reul, N., Plant, W., Stiassnie, M., Graber, H., Brown, O., Saltzman, E., 2004. On the limiting aerodynamic roughness of the ocean in very strong winds. Geophys. Res. Lett. 31, L18306. https://doi.org/10.1029/2004GL019460.

Draper, D.W., Long, D.G., 2004. Evaluating the effect of rain on SeaWinds scatterometer measurements. J. Geophys. Res. 109, C02005. https://doi.org/10.1029/2002JC001741.

Dvorak, V., 1984. Tropical cyclone intensity analysis using satellite data. NOAA Tech. Rep. NESDIS 11, 47. NOAA. https://satepsanone.nesdis.noaa.gov/pub/Publications/Tropical/Dvorak_1984.pdf. (Accessed 1 May 2020).

Elsberry, R.L., Harr, P.A., 2008. Tropical Cyclone Structure (TCS08) field experiment science basis, observational platforms, and strategy. Asia-Pac. J. Atmos. Sci. 44, 209−231.

Entekhabi, D., et al., 2004. The Hydrosphere State (HYDROS) mission: an Earth system pathfinder for global mapping of soil moisture and land freeze/thaw. IEEE Trans. Geosci. Remote Sens. 42, 2184−2195. https://doi.org/10.1109/TGRS.2004.834631.

Entekhabi, D., et al., 2014. SMAP Handbook. National Aeronautics and Space Administration, p. 192. https://smap.jpl.nasa.gov/system/internal_resources/details/original/178_SMAP_Handbook_FINAL_1_JULY_2014_Web.pdf. (Accessed 28 April 2020).

Entekhabi, D., Njoku, E., O'Neill, P., Kellogg, K.H., Crow, W., Edelstein, W.N., Entin, J., Goodman, S., Jackson, T., Johnson, J., Kimball, J., Piepmeier, J., Koster, R., Martin, N., McDonald, K., Moghaddam, M., Moran, S., Reichle, R., Shi, J., van Zyl, J., 2010. The soil moisture active passive (SMAP) mission. Proc. IEEE 98, 704−716. https://doi.org/10.1109/JPROC.2010.2043918.

Figa-Saldaña, J., Wilson, J.J.W., Attema, E., Gelsthorpe, R.V., Drinkwater, M.R., Stoffelen, A., 2002. The advanced scatterometer (ASCAT) on the meteorological operational (MetOp) platform: a follow on for European wind scatterometers. Can. J. Remote Sens. 28, 404−412. https://doi.org/10.5589/m02-035.

Fore, A.G., Stiles, B.W., Chau, A.H., Williams, B.A., Dunbar, R.S., Rodriguez, E., 2014. Point-wise wind retrieval and ambiguity removal improvements for the QuikSCAT climatological data set. IEEE Trans. Geosci. Remote Sens. 52, 51−59. https://doi.org/10.1109/TGRS.2012.2235843.

Fore, A.G., Yueh, S.H., Tang, W., Stiles, B.W., Hayashi, A.K., 2016. Combined active/passive retrievals of ocean vector wind and sea surface salinity with SMAP. IEEE Trans. Geosci. Remote Sens. 54, 7396−7404. https://doi.org/10.1109/TGRS.2016.2601486.

Fore, A.G., Yueh, S.H., Stiles, B.W., Tang, W., Hayashi, A.K., 2018. SMAP radiometer-only tropical cyclone intensity and size validation. IEEE Geosci. Remote Sens. Lett. 15, 1480−1484. https://doi.org/10.1109/LGRS.2018.2849649.

Fore, A.G., Yueh, S.H., Stiles, B.W., Tang, W., Hayashi, A.K., 2019. On extreme winds at L-band with the SMAP synthetic aperture radar. Remote Sens 11, 1093. https://doi.org/10.3390/rs11091093.

Franklin, J.L., Black, M.L., Valde, K., 2003. GPS dropwindsonde wind profiles in hurricanes and their operational implications. Weather Forecast. 18, 32−44. https://doi.org/10.1175/1520-0434(2003)018<0032:GDWPIH>2.0.CO;2.

Gaiser, P.W., Germain, K.S., Twarog, E.M., Poe, G.A., Purdy, W.E., Richardson, D., Grossman, W., Jones, W.L., Spencer, D., Golba, G., Cleveland, J., Choy, L., Bevilacqua, R.M., Chang, P.S., 2004. The WindSat spaceborne polarimetric microwave radiometer: sensor description and early orbit performance. IEEE Trans. Geosci. Remote Sens. 42, 2347−2361.

GEMS, 2020. IOD-1 GEMS (in orbit demonstration-1/global environmental monitoring satellite). https://directory.eoportal.org/web/eoportal/satellite-missions/i/iod-1-gems. (Accessed 18 June 2020).

Gohil, B.S., Sikhakolli, R., Gangwar, R.K., 2013. Development of geophysical model functions for Oceansat-2 scatterometer. IEEE Geosci. Remote Sens. Lett. 10, 377−380.

Gonzalez, F.I., Thompson, T.W., Brown, W.E., Weissman, D.E., 1982. SEASAT wind and wave observations of northeast Pacific hurricane Iva, August 13, 1978. J. Geophys. Res. 87, 3431−3438. https://doi.org/10.1029/JC087iC05p03431.

Graf, J., Sasaki, C., Winn, C., Liu, W.T., Tsai, W., Freilich, M., Long, D.G., 1998. NASA scatterometer experiment. Acta Astronaut. 43, 377−407. https://doi.org/10.1016/S0094-5765(97)00180-X.

Guard, C.P., Carr, L.E., Wells, F.H., Jeffries, R.A., Gural, N.D., Edson, D.K., 1992. Joint Typhoon Warning Center and the challenges of multibasin tropical cyclone forecasting. Weather Forecast. 7, 328−352. https://doi.org/10.1175/1520-0434(1992)007<0328:JTWCAT>2.0.CO;2.

Hagen, A.B., Landsea, C.W., 2012. On the classification of extreme Atlantic hurricanes utilizing mid-Twentieth-Century monitoring capabilities. J. Climate 25, 4461−4475.

Herndon, D., Velden, C., 2014. An update on tropical cyclone intensity estimation from satellite microwave sounders. In: 31st Conf. on Hurricanes and Tropical Meteorology. AMS, San Diego, CA, USA, p. 34. https://ams.confex.com/ams/31Hurr/webprogram/Paper244770.html.

Hilburn, K.A., Wentz, F.J., Smith, D.K., Ashcroft, P.D., 2006. Correcting active scatterometer data for the effects of rain using passive microwave data. J. Appl. Meteorol. Climatol. 45, 382−398. https://doi.org/10.1175/JAM2357.1.

Hock, T.F., Franklin, J.L., 1999. The NCAR GPS dropwindsonde. Bull. Amer. Meteor. Soc. 80, 407−420. https://doi.org/10.1175/1520-0477(1999)080<0407:TNGD>2.0.CO;2.

Holland, G.J., 1993. Ready reckoner. In: Neumann, C.J., Merrill, R.T., Jelesnianski, C.P., Gray, W.M., Foley, G.R., Southern, R.L., Puri, K., Holland, G.J. (Eds.), Report No. TCP-31 Global Guide to Tropical Cyclone Forecasting. WMO/TC-No. 560. WMO, Geneva, Switzerland, pp. 300−333. Available at: https://library.wmo.int/doc_num.php?explnum_id=9598.

Horstmann, J., Falchetti, S., Wackerman, C., Maresca, S., Caruso, M.J., Graber, H.C., 2015. Tropical cyclone winds retrieved from C-band cross-polarized synthetic aperture radar. IEEE Trans. Geosci. Remote Sens. 53, 2887−2898.

Hwang, P.A., Burrage, D., Wang, D., Wesson, J., 2013. Ocean surface roughness spectrum in high wind condition for microwave backscatter and emission computations. J. Atmos. Ocean. Tech. 30, 2168−2188. https://doi.org/10.1175/JTECH-D-12-00239.1.

Hwang, P.A., Fois, F., 2015. Surface roughness and breaking wave properties from polarimetric microwave radar backscattering. J. Geophys. Res. 120, 3640−3657. https://doi.org/10.1002/2015JC010782.

Hwang, P.A., Reul, N., Meissner, T., Yueh, S.H., 2019a. Whitecap and wind stress observations by microwave radiometers: global coverage and extreme conditions. J. Phys. Oceanogr. 49, 2291−2307. https://doi.org/10.1175/JPO-D-19-0061.1.

Hwang, P.A., Reul, N., Meissner, T., Yueh, S.H., 2019b. Ocean surface foam and microwave emission: dependence on frequency and incidence angle. IEEE Trans. Geosci. Remote Sens. 57, 8223−8234. https://doi.org/10.1109/TGRS.2019.2919001.

Hwang, P.A., Stoffelen, A., Van Zadelhoff, G.-J., Perrie, W., Zhang, B., Li, H., Shen, H., 2015. Cross-polarization geophysical model function for C-band radar backscattering from the ocean surface and wind speed retrieval. J. Geophys. Res.: Oceans 120, 893−909. https://doi.org/10.1002/2014JC010439.

Imaoka, K., Kachi, M., Kasahara, M., Ito, N., Nakagawa, K., Oki, T., 2010. Instrument performance and calibration of AMSR-E and AMSR2. Int. Arch. Photogramm. Remote Sens. Spat. Inf. Sci. 38, 13−16.

India Meteorological Department, 2021. Cyclone warning in India, Standard operation procedure [available online at: https://mausam.imd.gov.in/imd_latest/contents/pdf/cyclone_sop.pdf. .

Irish, J.L., Resio, D.T., Ratcliff, J.J., 2008. The influence of storm size on hurricane surge. J. Phys. Oceanogr. 38, 2003−2013. https://doi.org/10.1175/2008JPO3727.1.

Jma, 2020. Format of RSMC Best Track Data. National Typhoon Center, Japan Meteorological Agency. http://www.jma.go.jp/jma/jma-eng/jma-center/rsmc-hp-pub-eg/besttrack.html. (Accessed 20 April 2020).

Jones, W.L., Black, P.G., Delnore, V.E., Swift, C.T., 1981. Airborne microwave remote-sensing measurements in Hurricane Allen. Sci 214, 274−280.

JTWC, 1975. 1975 Annual Tropical Cyclone Report. US Fleet Weather Central, Joint Typhoon Warning Center, p. 85. https://www.metoc.navy.mil/jtwc/products/atcr/1975atcr.pdf. (Accessed 20 April 2020).

JTWC, 1989. 1989 Annual Tropical Cyclone Report. US Naval Oceanographic Command Center, Joint Typhoon Warning Center, p. 254. https://www.metoc.navy.mil/jtwc/products/atcr/1989atcr.pdf. (Accessed 29 June 2020).

JTWC, 1990. 1990 Annual Tropical Cyclone Report. US Naval Oceanographic Command Center, Joint Typhoon Warning Center, p. 278. https://www.metoc.navy.mil/jtwc/products/atcr/1990atcr.pdf. (Accessed 29 June 2020).

JTWC, 1992. 1992 Annual Tropical Cyclone Report. US Naval Oceanographic Command Center, Joint Typhoon Warning Center, p. 280. https://www.metoc.navy.mil/jtwc/products/atcr/1992atcr.pdf. (Accessed 29 June 2020).

JTWC, 2004. 2004 Annual Tropical Cyclone Report. US Naval Oceanographic Command Center, Joint Typhoon Warning Center, p. 327. https://www.metoc.navy.mil/jtwc/products/atcr/2004atcr.pdf. (Accessed 20 April 2020).

JTWC, 2016. 2016 Annual Tropical Cyclone Report. Joint Typhoon Warning Center, p. 122. https://www.metoc.navy.mil/jtwc/products/atcr/2016atcr.pdf. (Accessed 20 April 2020).

JTWC, 2019. Best track archive. https://www.metoc.navy.mil/jtwc/jtwc.html?best-tracks. (Accessed 20 April 2020).

Katsaros, K.B., Vachon, P.W., Black, P.G., Dodge, P.P., Uhlhorn, E.W., 2000. Wind fields from SAR: could they improve our understanding of storm dynamics? Johns Hopkins APL Tech. Dig. 21, 86−93.

Kawanishi, T., et al., 2003. The Advanced Microwave Scanning Radiometer for the Earth Observing System (AMSR-E), NASDA's contribution to the EOS for global energy and water cycle studies. IEEE Trans. Geosci. Remote Sens. 41, 184−194. https://doi.org/10.1109/TGRS.2002.808331.

Kerr, Y.H., et al., 2010. The SMOS Mission: new tool for monitoring key elements of the global water cycle. Proc. IEEE 98, 66−687. https://doi.org/10.1109/JPROC.2010.2043032.

Kilic, L., Prigent, C., Aires, F., Boutin, J., Heygster, G., Tonboe, R.T., Roquet, H., Jimenez, C., Donion, C., 2018. Expected performances of the Copernicus Imaging Microwave Radiometer (CIMR) for an all-weather and high spatial resolution estimation of ocean and sea ice parameters. J. Geophys. Res.: Oceans 123, 7564−7580. https://doi.org/10.1029/2018JC014408.

Kimball, S.K., Mulekar, M.S., 2004. A 15-year climatology of North Atlantic tropical cyclones. Part I: size parameters. J. Climate 17, 3555−3575. https://doi.org/10.1175/1520-0442(2004)017,3555. AYCONA.2.0.CO;2.

Klotz, B.W., Nolan, D.S., 2019. SFMR surface wind undersampling over the tropical cyclone life cycle. Mon. Weather Rev. 147, 247−268.

Klotz, B.W., Uhlhorn, E.W., 2014. Improved Stepped Frequency Microwave Radiometer tropical cyclone surface winds in heavy precipitation. J. Atmos. Oceanic Technol. 31, 2392–2408. https://doi.org/10.1175/JTECH-D-14-00028.1.

Knaff, J.A., Brown, D.P., Courtney, J., Gallina, G.M., Beven II, J.L., 2010. An evaluation of Dvorak Technique-based tropical cyclone intensity estimates. Weather Forecast. 25, 1362–1379.

Knaff, J.A., DeMaria, M., Molenar, D.A., Sampson, C.R., Seybold, M.G., 2011. An automated, objective, multi-satellite platform tropical cyclone surface wind analysis. J. Appl. Meteorol. Climatol. 50, 2149–2166. https://doi.org/10.1175/2011JAMC2673.1.

Knaff, J.A., Longmore, S.P., Molenar, D.A., 2014. An objective satellite-based tropical cyclone size climatology. J. Clim. 27, 455–476. https://doi.org/10.1175/JCLI-D-13-00096.1.

Knaff, J.A., Longmore, S.P., DeMaria, R.T., Molenar, D.A., 2015. Improved tropical-cyclone flight-level wind estimates using routine infrared satellite reconnaissance. J. Appl. Meteor. Climatol. 54, 463–478. https://doi.org/10.1175/JAMC-D-14-0112.1.

Knaff, J.A., Slocum, C.J., Musgrave, K.D., Sampson, C.R., Strahl, B.R., 2016. Using routinely available information to estimate tropical cyclone wind structure. Mon. Weather Rev. 144, 1233–1247.

Knapp, K.R., Kruk, M.C., Levinson, D.H., Diamond, H.J., Neumann, C.J., 2010. The international best track archive for climate stewardship (IBTrACS): unifying tropical cyclone best track data. Bull. Amer. Meteor. Soc. 91, 363–376. https://doi.org/10.1175/2009BAMS2755.1.

Knapp, Kenneth R., Diamond, Howard J., Kossin, James P., Kruk, Michael C., Schreck III, Carl J., 2018. International Best Track Archive for Climate Stewardship (IBTrACS) Project. Version 4. [Documentation]. NOAA National Centers for Environmental Information. https://doi.org/10.25921/82ty-9e16 [4/21/2021].

Koch, W., 2004. Directional analysis of SAR images aiming at wind direction. IEEE Trans. Geosci. Remote Sens. 42, 702–710. https://doi.org/10.1109/TGRS.2003.818811.

Kossin, J., Knaff, J., Berger, H., Herndon, D., Cram, T., Velden, C., Murnane, R., Hawkins, J., 2007. Estimating hurricane wind structure in the absence of aircraft reconnaissance. Weather Forecast. 22, 89–101. https://doi.org/10.1175/WAF985.1.

Landsea, C., Franklin, J., 2013. Atlantic hurricane database uncertainty and presentation of a new database format. Mon. Weather Rev. 141, 3576–3592. https://doi.org/10.1175/MWR-D-12-00254.1.

Lee, C., Cheung, K.K., Fang, W., Elsberry, R.L., 2010. Initial maintenance of tropical cyclone size in the western North Pacific. Mon. Weather Rev. 138, 3207–3223. https://doi.org/10.1175/2010MWR3023.1.

Lin, W., Portabella, M., Stoffelen, A., Verhoef, A., Wang, Z., 2018. Validation of the NSCAT-5 geophysical model function for SCATSAT-1 wind scatterometer. In: IGARSS 2018 - 2018 IEEE International Geoscience and Remote Sensing Symposium, pp. 3196–3199. https://doi.org/10.1109/IGARSS.2018.8517739. Valencia, Spain.

QuikSCAT science data product user's manual: overview and geophysical data products. v3.0. In: Lungu, T., Callahan, P.S. (Eds.), JPL Tech. Rep. 91.

Mallen, K.J., Montgomery, M.T., Wang, B., 2005. Reexamining the near-core radial structure of the tropical cyclone primary circulation: implications for vortex resiliency. J. Atmos. Sci. 62, 408–425. https://doi.org/10.1175/JAS-3377.1.

Manaster, A., Ricciardulli, L., Meissner, T., 2021. Tropical cyclone winds from WindSat, AMSR2, and SMAP: comparison with the HWRF model. Remote Sens 13, 2347. https://doi.org/10.3390/rs13122347, 2021.

Masters, D., Esterhuizen, S.X., Jales, P., Ibrahimi, E., Nogues-Correig, O., Yuasa, T., Nguyen, V., Irisov, V., Duly, T., Tan, L., 2019. First results from the Spire GNSS-R payload CubeSat missions. In: AGU Fall Meeting 2019. American Geophysical Union, San Francisco, CA, USA. Abstract #G14A-06.

Mecklenburg, S., Drusch, M., Kaleschke, L., Rodriguez-Fernandez, N., Reul, N., Kerr, Y.H., Font, J., Martin-Neira, M., Oliva, R., Daganzo-Eusebio, E., Grant, J.P., Sabia, R., Macelloni, G., Rautiainen, K., Fauste, J., de Rosnay, P., Munoz-Sabater, J., Verhoest, N., Lievens, H., Delwart, S., Crapolicchio, R., de la Fuente, A., Kornberg, M., 2016. ESA's Soil Moisture and Ocean Salinity mission: from science to operational applications. Remote Sens. Environ. 180, 3–18. https://doi.org/10.1016/j.rse.2015.12.025.

Meissner, T., Wentz, F., 2009. Wind vector retrievals under rain with passive satellite microwave radiometers. IEEE Trans. Geosci. Remote Sens. 47, 3065–3083.

Meissner, T., Wentz, F., Ricciardulli, L., 2014. The emission and scattering of L-band microwave radiation from rough ocean surfaces and wind speed measurements from the Aquarius sensor. J. Geophys. Res.: Oceans 119, 6499–6522. https://doi.org/10.1002/2014JC009837.

Meissner, T., Ricciardulli, L., Wentz, F.J., 2017. Capability of the SMAP mission to measure ocean surface winds in storms. Bull. Amer. Meteor. Soc. 98, 1660–1677. https://doi.org/10.1175/BAMS-D-16-0052.1.

Meissner, T., Ricciardulli, L., Manaster, A., 2021. Tropical cyclone wind speeds from WindSat, AMSR and SMAP: algorithm development and testing. Remote Sens 13, 1641. https://doi.org/10.3390/rs13091641.

Metzger, E.J., Hurlburt, H.E., Wallcraft, A.J., Shriver, J.F., Smedstad, L.F., Smedstad, O.M., Thoppil, P., Franklin, D.S., 2008. Validation test report for the global ocean prediction system V3.0 – 1/128 HYCOM/NCODA: phase I. NRL memo. Rep. NRL/MR/7320–08-9148. https://www.hycom.org/attachments/366_HYCOM-NCODA_VTR_I_Memo_Report_9148.pdf. (Accessed 1 July 2020).

Miller, R.J., Schrader, A.J., Sampson, C.R., Tsui, T.L., 1990. The automated tropical cyclone forecasting system. Weather Forecast. 5, 653–660.

Misra, T., Chakraborty, P., Lad, C., Gupta, P., Rao, J., Upadhyay, G., Kumar, S., Kumar, B., Gangele, S., Sinha, S., Tolani, H., Vithani, H.V., Raman, B., Rao, C., Dave, D., Jyoti, R., Desai, N., 2019. SCATSAT-1 Scatterometer: an improved successor of OSCAT. Current Sci 117, 941–949. https://doi.org/10.18520/cs/v117/i6/941-949 [available online at: https://wwwops.currentscience.ac.in/Volumes/117/06/0941.pdf.

Mohammed, P.N., Aksoy, M., Piepmeier, J.R., Johnson, J.T., Bringer, A., 2016. SMAP L-band microwave radiometer: RFI mitigation prelaunch analysis and first year on-orbit observations. IEEE Trans. Geosci. Remote Sens. 54, 6035–6047.

Monahan, E.C., O'Muircheartaigh, I., 1980. Optimal Power-Law Description of oceanic whitecap coverage dependence on wind speed. J. Phys. Oceanogr. 10, 2094–2099. https://doi.org/10.1175/1520-0485(1980)010<2094:OPLDOO>2.0.CO;2.

Monaldo, F., Kerbaol, V., Clemente-Colon, P., Furevik, B., Horstmann, J., Johannessen, J., Li, X., Pichel, W., Sikora, T., Thompson, D., Wackerman, C., 2003. The SAR measurement of ocean surface winds: an Overview. In: Proceedings of the Second Workshop on Coastal and Marine Applications of SAR (ESA SP-565). SeaSAR 2003, Svalbard, Norway, p. 18pp.

Morris, M., Ruf, C.S., 2017a. Estimating tropical cyclone integrated kinetic energy with the CYGNSS satellite constellation. J. Appl. Meteorol. Climatol. 56, 235–245. https://doi.org/10.1175/JAMC-D-16-0176.1.

Morris, M., Ruf, C.S., 2017b. Determining tropical cyclone surface wind speed structure and intensity with the CYGNSS satellite constellation. J. Appl. Meteorol. Climatol. 56, 1847–1865. https://doi.org/10.1175/JAMC-D-16-0375.1.

Mouche, A., Chapron, B., Zhang, B., Husson, R., 2017. Combined co- and cross- polarized SAR measurements under extreme wind conditions. IEEE Trans. Geosci. Remote Sens. 55, 6746–6755. https://doi.org/10.1109/TGRS.2017.2732508.

Mouche, A., Chapron, B., Knaff, J., Zhao, Y., Zhang, B., Combot, C., 2019. Co- and Cross- polarized SAR measurements for high-resolution description of major hurricane wind-structures: application to Irma category-5 Hurricane. J. Geophy. Res.: Oceans 124, 3905–3922. https://doi.org/10.1029/2019JC015056.

NASA, 1978. Seasat – 1. https://nssdc.gsfc.nasa.gov/nmc/spacecraft/display.action?id=1978-064A. (Accessed 1 May 2020).

NASA, 2020. What Are SmallSats and CubeSats? https://www.nasa.gov/content/what-are-smallsats-and-cubesats. (Accessed 9 July 2020).

Needham, H.F., Keim, B.D., 2014. An empirical analysis on the relationship between tropical cyclone size and storm surge heights along the U.S. Gulf Coast. Earth Interact. 18, 1–15. https://doi.org/10.1175/2013EI000558.1.

NHC, 2019. 2. Forecast verification procedures. https://www.nhc.noaa.gov/verification/verify2.shtml. (Accessed 30 March 2019).

NHC, 2020. Tropical cyclone forecast/advisory (TCM) - how to read. https://www.nhc.noaa.gov/aboutnhcprod.shtml#TCM. (Accessed 27 July 2020).

Nordberg, W., Conaway, J., Ross, D.B., Wilheit, T., 1971. Measurements of microwave emission from a foam-covered, wind-driven sea. J. Atmos. Sci. 28, 429–435. https://doi.org/10.1175/1520-0469(1971)028<0429:MOMEFA>2.0.CO;2.

OEPortal, 2020. WSF-M (weather system follow-on - microwave) satellite. https://directory.eoportal.org/web/eoportal/satellite-missions/content/-/article/wsf-m. (Accessed 27 May 2020).

OFCM, 2019. National hurricane Operation Plan. FCM-P12-2019. Office of the Federal Coordinator for Meteorological Services and Supporting Research, Washington, DC, p. 176. https://www.ofcm.gov/publications/nhop/fcm-p12-2019.pdf. (Accessed 23 April 2020).

Olander, T.L., Velden, C.S., 2019. The Advanced Dvorak Technique (ADT) for estimating tropical cyclone intensity: update and new capabilities. Weather Forecast. 34, 905–922. https://doi.org/10.1175/WAF-D-19-0007.1.

OMAO, 2020. Lockeed WP-3 orion. https://www.omao.noaa.gov/learn/aircraft-operations/aircraft/lockheed-wp-3d-orion. (Accessed 1 May 2020).

Piñeros, M.F., Ritchie, E.A., Tyo, J.S., 2008. Objective measures of tropical cyclone structure and intensity change from remotely-sensed infrared image data. IEEE Trans. Geosci. Remote Sens. 46, 3574–3580. https://doi.org/10.1109/TGRS.2008.2000819.

Piñeros, M.F., Ritchie, E.A., Tyo, J.S., 2010. Detecting tropical cyclone genesis from remotely-sensed infrared image data. IEEE Trans. Geosci. Remote Sens. Lett. 7, 826–830. https://doi.org/10.1109/LGRS.2010.2048694.

Portabella, M., Stoffelen, A., Lin, W., Turiel, A., Verhoef, A., Verspeek, J., Ballabera-Poy, J., 2012. Rain effects on ASCAT-retrieved winds: toward an improved quality control. IEEE Trans. Geosci. Remote Sens. 50, 2495–2506. https://doi.org/10.1109/TGRS.2012.2185933.

Powell, M.D., Houston, S.H., Amat, L.R., Morisseau-Leroy, N., 1998. The HRD real-time hurricane wind analysis system. J. Wind Eng. Ind. Aerodyn. 77–78, 53–64. https://doi.org/10.1016/S0167-6105(98)00131-7.

Powell, M.D., Reinhold, T.A., 2007. Tropical cyclone destructive potential by integrated kinetic energy. Bull. Amer. Meteor. Soc. 88, 513–526. https://doi.org/10.1175/BAMS-88-4-513.

Rappaport, E.N., Franklin, J.L., Avila, L.A., Baig, S.R., Beven, J.L., II, Blake, E.S., Burr, C.A., Jiing, J., Juckins, C.A., Knabb, R.D., Landsea, C.W., Mainelli, M., Mayfield, M., McAdie, C.J., Pasch, R.J., Sisko, C., Stewart, S.R., Tribble, A.N., 2009. Advances and challenges at the national hurricane center. Weather Forecast. 24, 395–419.

Reade, D., 2014. The resurgence of tropical cyclone reconnaissance aircraft in the Far East and Western Pacific. P-3 Publications, p. 34. http://p-3publications.com/PDF/ResurgenceofTropicalCycloneReconnaissanceAircraft.pdf. (Accessed 2 July 2020).

Reul, N., Chapron, B., 2003. A model of sea-foam thickness distribution for passive microwave remote sensing applications. J. Geophys. Res. 108 (C10), 3321. https://doi.org/10.1029/2003JC001887.

Reul, N., Tenerelli, J., Chapron, B., Vandemark, D., Quilfen, Y., Kerr, Y., 2012. SMOS satellite L-band radiometer: a new capability for ocean surface remote sensing in hurricanes. J. Geophys. Res. 117, C02006. https://doi.org/10.1029/2011JC007474.

Reul, N., Chapron, B., Zabolotskikh, E., Donlon, C., Mouche, A., Tenerelli, J., Collard, F., Piolle, J.F., Fore, A., Yueh, S., Cotton, J., Francis, P., Quilfen, Y., Kudryavtsev, V., 2017. A new generation of tropical cyclone size measurements from space. Bull. Amer. Meteor. Soc. 98, 2367–2385. https://doi.org/10.1175/BAMS-D-15-00291.1.

Reul, N., Chapron, B., Zabolotskikh, E., Donlon, C., Quilfen, Y., Guimbard, S., Piolle, J.F., 2016. A revised L-band radio-brightness sensitivity to extreme winds under tropical cyclones: the five year SMOS-storm database. Remote Sens. Environ. 180, 274–291. https://doi.org/10.1016/j.rse.2016.03.011.

Ricciardulli, L., Wentz, F., 2015. A scatterometer geophysical model function for climate-quality winds: QuikSCAT Ku-2011. J. Atmos. Oceanic Technol. 32, 1829–1846. https://doi.org/10.1175/JTECH-D-15-0008.1.

Rosen, P., Hensley, S., Shaffer, S., Edelstein, W., Kim, Y., Kumar, R., Misra, T., Bhan, R., Sagi, R., 2017. The NASA-ISRO SAR (NISAR) mission dual-band radar instrument preliminary design. In: 2017 IEEE International Geoscience and Remote Sensing Symposium (IGARSS), pp. 3832–3835. https://doi.org/10.1109/IGARSS.2017.8127836. Fort Worth, TX, USA.

Rostan, F., Ulrich, D., Heer, C., Østergaard, A., 2019. The Metop-Sg Sca wind Scatterometer: cdr development status and performance overview. In: IGARSS 2019 - 2019 IEEE International Geoscience and Remote Sensing Symposium, pp. 8332–8335. https://doi.org/10.1109/IGARSS.2019.8898784. Yokohama, Japan.

Ruf, C.S., Atlas, R., Chang, P.S., Clarizia, M.P., Garrison, J.L., Gleason, S., Katzberg, S.J., Jelenak, Z., Johnson, J.T., Majumdar, S.J., O'Brien, A., Posselt, D.J., Ridley, A.J., Rose, R.J., Zavorotny, V.U., 2016a. New ocean winds satellite mission to probe hurricanes and tropical convection. Bull. Amer. Meteor. Soc. 97, 385–395. https://doi.org/10.1175/BAMS-D-14-00218.1.

Ruf, C., Chang, P., Clarizia, M.P., Gleason, S., Jelenak, Z., Murray, J., Morris, M., Musko, S., Posselt, D., Provost, D., Starkenburg, D., Zavorotny, V., 2016b. CYGNSS Handbook Cyclone Global Navigation Satellite System: Deriving Surface Wind Speeds in Tropical Cyclones, first ed. Michigan Publishing, Ann Arbor, MI.

Ruf, C., Balasubramaniam, R., 2018. Development of the CYGNSS geophysical model function for wind speed. IEEE J. Sel. Topics Appl. Earth Obs. Remote Sens. 12, 66–77. https://doi.org/10.1109/JSTARS.2018.2833075.

Ruf, C., Gleason, S., McKague, D.S., 2019. Assessment of CYGNSS wind speed retrieval uncertainty. IEEE J. Sel. Topics Appl. Earth Obs. Remote Sens. 12, 87–97. https://doi.org/10.1109/JSTARS.2018.2825948.

Rupp, J.A., Lander, M.A., 1996. A technique for estimating recurrence intervals of tropical cyclone–related high winds in the Tropics: results for Guam. J. Appl. Meteor. 35, 627–637.

Sampson, C.R., Schrader, A.J., 2000. The automated tropical cyclone forecasting system (version 3.2). Bull. Amer. Meteor. Soc. 81, 1231–1240.

Sampson, C., Fukada, E., Knaff, J.A., Strahl, B., Brennan, M., Marchok, T., 2017. Tropical cyclone gale wind radii estimates for the western North Pacific. Weather Forecast. 32, 1029–1040. https://doi.org/10.1175/WAF-D-16-0196.1.

Sampson, C.R., Goerss, J.S., Knaff, J.A., Strahl, B.R., Fukada, E.M., Serra, E.A., 2018. Tropical cyclone gale wind radii estimates, forecasts and error forecast for the western North Pacific. Weather Forecast. 33, 1081–1092. https://doi.org/10.1175/WAF-D-17-0153.1.

Sapp, J., Alsweiss, S., Jelenak, Z., Chang, P., Frasier, S., Carswell, J., 2016. Airborne co-polarization observations of the ocean-surface NRCS at C-band. IEEE Trans. Geosci. Rem. Sens. 54, 5975–5992. https://doi.org/10.1109/TGRS.2016.2578048.

Sapp, J.W., Alsweiss, S.O., Jelenak, Z., Chang, P.S., Carswell, J., 2019. Stepped frequency microwave radiometer wind-speed retrieval improvements. Remote Sens 11, 214. https://doi.org/10.3390/rs11030214.

Schubert, W.H., Montgomery, M.T., Taft, R.K., Guinn, T.A., Fulton, S.R., Kossin, J.P., Edwards, J.P., 1999. Polygonal eyewalls, asymmetric eye contraction, and potential vorticity mixing in hurricanes. J. Atmos. Sci. 56, 1197–1223. https://doi.org/10.1175/1520-0469(1999)056<1197:PEAECA>2.0.CO;2.

SeaPAC, 2013. QuikSCAT level 2B ocean wind vectors in 12.5km slice composites version 3. PO.DAAC v3. https://doi.org/10.5067/QSX12-L2B01. (Accessed 4 May 2020).

Sheets, R.C., 1990. The National Hurricane Center—past, present, and future. Weather Forecast. 5, 185–232.

Shibata, A., 2002. Chapter 8: AMSR/AMSR-E sea surface wind speed algorithm. EORC Bulletin/Technical Report 9, 2. https://sharaku.eorc.jaxa.jp/AMSR/doc/alg/8_alg.pdf. (Accessed 29 June 2020).

Shibata, A., 2006. A wind speed retrieval algorithm by combining 6 and 10 GHz data from Advanced Microwave Scanning Radiometer: wind speed inside hurricanes. J. Oceanogr. 62, 351–359.

Soisuvarn, S., Jelenak, Z., Chang, P.S., Alsweiss, S.O., Zhu, Q., 2013. CMOD5.H—a high wind geophysical model function for C-band vertically polarized satellite scatterometer measurements. IEEE Trans. Geosci.

Remote Sens. 51, 3744−3760. https://doi.org/10.1109/TGRS.2012.2219871.
Soldo, Y., Khazaal, A., Cabot, F., Kerr, Y.H., 2015. An RFI index to quantify the contamination of SMOS data by radio-frequency interference. IEEE J. Sel. Topics Appl. Earth Obs. Remote Sens. 9, 1577−1589.
Stiles, B.W., Yueh, S.H., 2002. Impact of rain on spaceborne Ku-band wind scatterometer data. IEEE Trans. Geosci. Remote Sens. 40, 1973−1983. https://doi.org/10.1109/TGRS.2002.803846.
Stiles, B.W., Danielson, R.E., Poulsen, W.L., Brennan, M.J., Hristova-Veleva, S., Shen, T.-P., Fore, A.G., 2014. Optimized tropical cyclone winds from QuikSCAT: a neural network approach. IEEE Trans. Geosci. Remote Sens. 52, 7418−7434. https://doi.org/10.1109/TGRS.2014.2312333.
Stoffelen, A., 1998. Scatterometry. Ph.D. Dissertation. University of Utrecht, Utrecht, Netherlands, p. 209. https://dspace.library.uu.nl/bitstream/handle/1874/636/full.pdf. (Accessed 4 May 2020).
Stoffelen, A., Verspeek, J., Vogelzang, J., Verhoef, A., 2017a. The CMOD7 geophysical model function for ASCAT and ERS wind retrievals. IEEE J. Sel. Topics Appl. Earth Obs. Remote Sens. 10, 2123−2134. https://doi.org/10.1109/JSTARS.2017.2681806.
Stoffelen, A., Aaboe, S., Calvet, J.-C., Cotton, J., Chiara, G.D., Saldana, J.F., Mouche, A.A., Portabella, M., Scipal, K., Wolfgang, W., 2017b. Scientific developments and the EPS-SG scatterometer. IEEE J. Sel. Topics Appl. Earth Obs. Remote Sens. 10, 2086−2097. https://doi.org/10.1109/JSTARS.2017.2696424.
Tachi, K., Arai, K., Sato, Y., 1989. Advanced microwave scanning radiometer (AMSR): requirements and preliminary design study. IEEE Trans. Geosci. Remote Sens. 27, 177−183. https://doi.org/10.1109/36.20296.
Thompson, A.A., 2015. Overview of the RADARSAT constellation mission. Canadian J. Remote Sens. 41, 401−440. https://doi.org/10.1080/07038992.2015.1104633.
Tournadre, J., Quilfen, Y., 2003. Impact of rain cell on scatterometer data: theory and modeling. J. Geophys. Res. 108, 3225−3238. https://doi.org/10.1029/2002JC001428.
Torn, R.D., Snyder, C., 2012. Uncertainty of tropical cyclone best-track information. Weather Forecast. 27, 715−729. https://doi.org/10.1175/WAF-D-11-00085.1.
T-PARC, 2008. THORPEX (THe observing research and predictability EXperiment) pacific asian regional Campaign (T-PARC). https://www.eol.ucar.edu/field_projects/t-parc. (Accessed 23 April 2020).
TROPICS, 2019. Time-Resolved Observations of Precipitation Structure and Storm Intensity with a Constellation of Smallsats. Factsheet, p. 2. https://tropics.ll.mit.edu/CMS/tropics/pdf/nasaTropicsFactSheet.pdf. (Accessed 27 May 2020).
Uhlhorn, E.W., Black, P.G., 2003. Verification of remotely sensed sea surface winds in hurricanes. J. Atmos. Oceanic. Tech. 20, 99−116.
Uhlhorn, E.W., Nolan, D.S., 2012. Observational undersampling in tropical cyclones and implications for estimated intensity. Mon. Weather Rev. 140, 825−840.
Uhlhorn, E.W., Black, P.G., Franklin, J.L., Goodberlet, M., Carswell, J., Goldstein, A.S., 2007. Hurricane surface wind measurements from an operational stepped frequency microwave radiometer. Mon. Weather Rev. 135, 3070−3085.
Velden, C.S., Herndon, D., 2020. A consensus approach for estimating tropical cyclone intensity from meteorological satellites: SATCON. Weather Forecast. 35, 1645−1662. https://doi.org/10.1175/WAF-D-20-0015.1.
Velden, C.S., et al., 2006. The Dvorak tropical cyclone intensity estimation technique: a satellite-based method that has endured for over 30 years. Bull. Amer. Meteor. Soc. 87, 1195−1210. https://doi.org/10.1175/BAMS-87-9-1195.
Verspeek, J., Stoffelen, A., Portabella, M., Bonekamp, H., Anderson, C., Figa-Saldana, J., 2010. Validation and calibration of ASCAT using CMOD5. IEEE Trans. Geosci. Remote Sens. 48, 386−395.
Vigh, J.L., Knaff, J.A., Schubert, W.H., 2012. A climatology of hurricane eye formation. Mon. Weather Rev. 140, 1405−1426. https://doi.org/10.1175/MWR-D-11-00108.1.
Wang, H., Zhu, J., Lin, M., Zhang, Y., Chang, Y., 2020. Evaluating Chinese HY-2B HSCAT ocean wind products using buoys and other scatterometers. Geosci. Rem. Sens. Lett. IEEE 17, 923−927. https://doi.org/10.1109/LGRS.2019.2940384.
Weatherford, C.L., Gray, W.M., 1988. Typhoon structure as revealed by aircraft reconnaissance. Part I: data analysis and climatology. Mon. Weather Rev. 116, 1032−1043.
Wentz, F., 2005. The effects of cloud and rain on the aquarius salinity retrieval. RSS technical report 3031805, remote sensing systems. Santa Rosa, California. http://images.remss.com/papers/rsstech/2005_3031805_Wentz_rain_effect_on_salinity.pdf. (Accessed 29 June 2020).
Wentz, F.J., Smith, D.K., 1999. A model function for the ocean-normalized radar cross section at 14 GHz derived from NSCAT observations. J. Geophys. Res. 104, 11499−11514. https://doi.org/10.1029/98JC02148.
Weissman, D.E., Bourassa, M.A., 2008. Measurements of the effect of rain-induced sea surface roughness on the QuikSCAT scatterometer radar cross section. IEEE Trans. Geosci. Remote Sens. 46, 2882−2894. https://doi.org/10.1109/TGRS.2008.2001032.
Williams, J., 2015. Into the eye: tracing the history of the hurricane hunters. Weatherwise 68, 37−45. https://doi.org/10.1080/00431672.2015.1067110.
Wimmers, A., Velden, C., Cossuth, J., 2019. Using deep learning to estimate tropical cyclone intensity from satellite passive microwave imagery. Mon. Weather Rev. 147, 2261−2282. https://doi.org/10.1175/MWR-D-18-0391.1.
Wong, W.K., Tse, S.M., Chan, P.W., 2014. Impacts of reconnaissance flight data on numerical simulation of tropical cyclones over South China Sea. Meteorol. Appl. 21, 831−847. https://doi.org/10.1002/met.1412.
Wu, C.-C., Lin, P.-H., Aberson, S., Yeh, T.-C., Huang, W.-P., Chou, K.-H., Hong, J.-S., Lu, G.-C., Fong, C.-T., Hsu, K.-C., Lin, I.-I., Lin, P.-L., Liu, C.-H., 2005. Dropsonde observations for typhoon surveillance near the Taiwan region (DOTSTAR): an overview. Bull. Amer. Meteorol. Soc. 86, 787−790.
Yamada, H., Tsuboki, K., Nagahama, N., Shimizu, K., Ohigashi, T., Shinoda, T., Ito, K., Yamaguchi, M., Nakazawa, T., 2018. Double warm-core structure of Typhoon Lan (2017) as observed through upper-tropospheric aircraft reconnaissance during T-PARCII. In: 33rd Conf. on Hurricanes and Tropical Meteorology. AMS, Ponte Verde, FL. Available at: https://ams.confex.com/ams/33HURRICANE/webprogram/Manuscript/Paper339931/201804_HurricaneConf_Yamada_extendAbst.pdf.
Yueh, S.H., Tang, W., Fore, A.G., Neumann, G., Hayashi, A., Freedman, A., Chaubell, J., Lagerloef, G.S.E., 2013. L-band passive and active microwave geophysical model functions of ocean surface winds and applications to aquarius retrieval. IEEE Trans. Geosci. Remote Sens. 51, 4619−4632. https://doi.org/10.1109/TGRS.2013.2266915.
Yueh, S., Fore, A., Tang, W., Hayashi, A., Stiles, B., Reul, N., Wengi, Y., Zhang, F., 2016. SMAP L-band passive microwave observations of ocean surface wind during severe storms. IEEE Trans. Geosci. Remote Sens. 54, 7339−7350. https://doi.org/10.1109/TGRS.2016.2600239.
Zabolotskikh, E., Mitnik, L., Reul, N., Chapron, B., 2015. New possibilities for geophysical parameter retrievals opened by GCOM-W1 AMSR2. IEEE J. Sel. Topics Appl. Earth Obs. Remote Sens. 8, 4248−4261. https://doi.org/10.1109/JSTARS.2015.2416514.
Zavorotny, V.U., Gleason, S., Cardellach, E., Camps, A., 2014. Tutorial on remote sensing using GNSS bistatic radar of opportunity. IEEE Geosci. Remote Sens. 2, 8−45. https://doi.org/10.1109/MGRS.2014.2374220.
Zhang, B., Perrie, W., Vachon, P.W., Li, X., Pichel, W.G., Guo, J., He, Y., 2012. Ocean vector winds retrieval from C-band fully polarimetric SAR measurements. IEEE Trans. Geosci. Remote Sens. 50, 4252−4426. https://doi.org/10.1109/TGRS.2012.2194157.
Zhao, A., Sun, R., Zhao, C., 2016. Application of HY-2A/SCAT sea surface winds in understanding structure of typhoons over Northwestern Pacific Ocean. In: Proceedings of the 4th International Workshop on Earth Observation and Remote Sensing Applications (EORSA) 2016, pp. 72−77. https://doi.org/10.1109/EORSA.2016.7552769. Guangzhou, China.
Zhao, K., Zhao, C., 2019. Evaluation of HY-2A Scatterometer ocean surface wind data during 2012−2018. Remote Sens 11, 2968. https://doi.org/10.3390/rs11242968.